

Insights into solid-waste management of poly(1,4-butylene adipate-co-1,4-butylene terephthalate): Degradation behavior under model industrial conditions

Item Type	Journal article
Authors	Sikorska, Wanda;Duale, Khadar;Musioł, Marta;Janeczek, Henryk;Hercog, Anna;Olszowska, Karolina;Marcinkowski, Andrzej;Andrä-Żmuda, Silke;Godzierz, Marcin;Pławszewska, Marzena;Puskas, Judit E.;Michel, Frederick C.;Klingman, Michael;Focarete, Maria Letizia;Fray, Mirosława El;Gorący, Krzysztof;Walkowiak, Konrad;Rokicka, Joanna;Niedźwiedź, Malwina;Radecka, Iza;Gupta, Abhishek;Kowalczyk, Marek;Rydz, Joanna
Citation	Sikorska, W., Duale, K., Musioł, M. et al.(2026) Insights into solid-waste management of poly(1,4-butylene adipate-co-1,4-butylene terephthalate): Degradation behavior under model industrial conditions. <i>Polymer Degradation and Stability</i> , 249, 112125.
DOI	10.1016/j.polymdegradstab.2026.112125
Publisher	Elsevier
Journal	<i>Polymer Degradation and Stability</i>
Download date	2026-06-08 05:55:10
License	https://creativecommons.org/licenses/by-nc-nd/4.0/
Link to Item	https://wlv.openrepository.com/handle/2436/626315

1 **Insights into solid-waste management of poly(1,4-butylene adipate-co-1,4-butylene**
2 **terephthalate): Degradation behavior under model industrial conditions**

3

4 Wanda Sikorska*¹, Khadar Duale¹, Marta Musioł¹, Henryk Janeczek¹, Anna Hercog^{1,2},
5 Karolina Olszowska¹, Andrzej Marcinkowski¹, Silke Andrä-Żmuda¹, Marcin Godzierz¹,
6 Marzena Pławszewska¹, Judit E. Puskas³, Frederick C. Michel Jr.⁴, Michael Klingman⁴, Maria
7 Letizia Focarete⁵, Mirosława El Fray⁶, Krzysztof Gorący⁶, Konrad Walkowiak⁶, Joanna
8 Rokicka⁶, Malwina Niedźwiedź⁶, Iza Radecka⁷, Abhishek Gupta⁷, Marek Kowalczyk¹ and
9 Joanna Rydz*¹

10 ¹Centre of Polymer and Carbon Materials Polish Academy of Sciences, M. Curie-Skłodowskiej
11 34, 41-819 Zabrze, Poland

12 ²SPIN-Lab Centre for Microscopic Research on Matter, University of Silesia in Katowice, 75
13 Pułku Piechoty 1A, 41-500 Chorzów, Poland

14 ³Department of Food, Agricultural and Biological Engineering, College of Food, Agricultural,
15 and Environmental Sciences, The Ohio State University, 1680 Madison Avenue, Wooster, OH
16 44691, United States

17 ⁴Department of Food, Agricultural and Biological Engineering, Ohio Agricultural Research and
18 Development Center, The Ohio State University, 1680 Madison Avenue, Wooster, OH 44691,
19 United States

20 ⁵Department of Chemistry “Giacomo Ciamician” and INSTM UdR of Bologna, University of
21 Bologna, via Gobetti 85, 40129, Bologna, Italy

22 ⁶Department of Polymer and Biomaterials Science, West Pomeranian University of Technology
23 in Szczecin, Al. Piastów 45, 70-311 Szczecin, Poland

24 ⁷School of Pharmacy and Life Sciences, Faculty of Science and Engineering, University of
25 Wolverhampton, Wulfruna St., Wolverhampton WV1 1LY, UK

26 Corresponding Author: *E-mail address: wsikorska@cmpw-pan.pl (W. Sikorska, ORCID
27 0000-0002-5651-8859), jrydz@cmpw-pan.pl (J. Rydz, ORCID 0000-0003-3972-7074)

28 **Dedicated to the late Ing. Dr. Henryk Janeczek, a passionate scientist, valued colleague**
29 **and dear friend**

30 **Abstract**

31 In this study, a comprehensive comparison of degradation dynamics across different
32 environments of the aliphatic-aromatic copolyester poly(1,4-butylene adipate-*co*-1,4-butylene
33 terephthalate) (PBAT), commercially known as Ecoflex[®], is presented. Effective solid-waste
34 management *via* organic recycling of biodegradable polymer waste requires a thorough
35 understanding of both their aerobic and anaerobic degradation processes. The results of
36 degradation studies on PBAT-based films, solvent-cast and pressed/molded – with and without
37 the addition of randomly methylated β -cyclodextrin (RM- β -CD), under model industrial
38 conditions: aerobic composting, anaerobic digestion, and hydrolytic degradation (used as a
39 reference process) were discussed. The inclusive assessment of morphological and
40 physicochemical changes provided valuable insight into the degradation dynamics of PBAT-
41 based films under model industrial conditions which constitutes a central and novel contribution
42 of this study. Furthermore, the careful selection of model systems played a crucial role in
43 enabling the evaluation of the influence of RM- β -CD on key polymer properties, such as
44 degradability and crystallinity. The findings demonstrate that the degradation profile of PBAT
45 can be modulated by adjusting the production method and/or incorporating suitable additives.
46 Furthermore, effective plastic waste management and the selection of appropriate composting
47 strategies remain essential to minimizing environmental impact.

48 **KEY WORDS**

49 aliphatic-aromatic copolyester, Ecoflex[®], PBAT, aerobic composting, anaerobic digestion,
50 hydrolytic degradation, randomly methylated β -cyclodextrin

51 **1. Introduction**

52 Biodegradable polymers are increasingly considered as alternatives to conventional plastics,
53 particularly in applications such as packaging and agricultural films. Within the framework of
54 solid-waste management, as defined by European Union (EU) directives (2008/98/EC and
55 2018/851), strategies such as waste separation, recycling, and resource recovery play a key role
56 in reducing environmental impact. In this context, biodegradable materials with well-defined
57 degradation behavior can be integrated into these systems, as they can decompose under
58 appropriate conditions into simpler compounds, thereby contributing to nutrient cycling in the
59 environment [1]. Biodegradability refers to the ability of a material to be broken down by
60 biological agents, such as bacteria and fungi, under natural conditions. The term
61 (bio)degradable is used to indicate that a material can be broken down either through abiotic
62 processes, such as simple hydrolysis, or through biological agents.

63 This characteristic contrasts significantly with non-biodegradable materials, which persist in
64 the environment for much longer periods. Products made from biodegradable polymers can,
65 after fulfilling their intended functions, undergo organic recycling in accordance with proper
66 solid-waste management principles [2–5]. Among biodegradable polymers, poly(1,4-butylene
67 adipate-*co*-1,4-butylene terephthalate) (PBAT) is a widely used aliphatic-aromatic copolyester
68 that exhibits desirable properties such as high flexibility, excellent processability, and
69 compatibility with conventional polymer processing equipment [6–9]. Recent studies have
70 focused on modifying PBAT with functional additives to tailor its properties but also its
71 degradation behavior. Among potential additives, cyclodextrins (CDs), including random
72 methyl- β -cyclodextrin (RM- β -CD), have emerged as promising candidates due to their unique
73 structure and ability to interact with polymer matrices, potentially affecting crystallinity,
74 thermal properties, and degradation processes [10–15]. However, despite these studies, the
75 effect of RM- β -CD on the degradation behavior of PBAT, particularly in relation to different

76 film preparation methods, has not been fully elucidated. Taking all factors into account,
77 understanding the degradation processes of biodegradable materials is essential for effective
78 solid-waste management in line with EU directives [16,17]. In this regard, this study aims to
79 critically assess and comprehensively compare the degradation dynamics of PBAT-based films
80 under model industrial systems, including aerobic composting, anaerobic digestion, and
81 hydrolytic conditions as a reference. In particular, the work evaluates the influence of the
82 fabrication method (solvent-cast vs. pressed and molded) and the presence of RM- β -CD on the
83 degradation behavior. For this purpose, controlled degradation experiments were performed on
84 multiple types of samples, and the materials were characterized before and after degradation
85 using optical microscopy (OM), scanning electron microscopy (SEM), atomic force
86 microscopy (AFM), gel permeation chromatography (GPC), nuclear magnetic resonance
87 (NMR), differential scanning calorimetry (DSC), X-ray diffraction (XRD) and
88 thermogravimetric analysis (TGA). This comprehensive analytical approach enabled a detailed
89 assessment of physicochemical properties, in particular changes in morphology, crystallinity,
90 and also provided insight into the degradation profiles of PBAT-based films under different
91 conditions. It also enabled the determination of the influence of RM- β -CD addition and film
92 fabrication method on the properties of the PBAT matrix. We hypothesize that the incorporation
93 of RM- β -CD and the selection of film processing methods can be used to tailor the degradation
94 behavior of PBAT-based films without adversely affecting their suitability for organic recycling
95 under industrial conditions.

96 **2. Materials and Methods**

97 *2.1. Materials*

98 Random methyl- β -cyclodextrin (RM- β -CD, DS ~12, CycloLab Ltd, Hungary) was used as
99 received. PBAT pellets (Ecoflex[®] Batch AB1 [18], BASF, Germany, and Ecoflex[®] F BX 7011,
100 Songhan Plastic Technology Co., Ltd, China) were employed as the polymer matrix.

101 Microcrystalline cellulose (50 μm , ThermoScientific Chemicals, US) was used as a positive
102 control in the anaerobic digestion experiment.

103 *2.2. Film preparation*

104 Solvent-cast PBAT (Ecoflex[®] Batch AB1) films were prepared by dissolving pellets in
105 chloroform (10 wt%) and casting the solution onto Teflon[®] discs. Films without RM- β -CD were
106 labeled EF, while films with 0.5 wt% RM- β -CD added to the solution were labeled EFCD.
107 Pressed films were obtained by stacking two solvent-cast films and pressing them at 110 °C
108 under 5 t for 1 min, according to the procedure previously established for pressed films (see
109 publications [14,15,19,20]); pressed films without RM- β -CD were labeled PEF, and those with
110 RM- β -CD added between two layers before pressing, following the procedure [14,15] were
111 labeled PEFC. Molded PBAT films (MEF) were injection-molded from Ecoflex F BX 7011
112 pellets using a BOY XS micro-injection molding machine (Dr. Boy GmbH & Co. KG,
113 Germany) at 110 and 120 °C in heating zones 1 and 2 °C, 60 bar, and 23 s in a single injection
114 cycle, with a room-temperature mold. Resulting films were 35 \times 35 mm, 0.5 mm thick, and
115 have average mass of 0.8 g.

116 *2.3. Antimicrobial activity and in vitro cytocompatibility tests*

117 Gram-negative *Escherichia coli* (K12W-T) and Gram-positive *Staphylococcus aureus*
118 (NCIMB 6571) from the University of Wolverhampton, UK culture collection were used for
119 antimicrobial assays. Cytotoxicity of pressed PBAT and PBAT/RM- β -CD films on mammalian
120 fibroblasts (MRC-5, Medical Research Council cell strain 5, fetal lung fibroblasts) was assessed
121 using the standard MTT (3-(4,5-dimethyl-1,3-thiazol-2-yl)-2,5-diphenyl-2H-tetrazol-3-ium
122 bromide) assay (Sigma, UK) as described previously [15].

123 *2.4. Hydrolytic degradation experiment*

124 The discs, with an average mass $m = 0.08 \pm 0.02$ mg for pressed PBAT films and $m = 0.14 \pm$
125 0.02 mg for pressed PBAT/RM- β -CD films, and a diameter of 2.0 ± 0.02 cm, were subjected

126 to incubation in screw-top bottles containing 25 ml of demineralized water (initial pH = 6.7) at
127 temperature of 37 and 70 °C (± 0.5 °C), in accordance with International Standard ISO
128 13781:2017 [21]. Following the specified period of degradation (7, 21, 42, and 70 days), the
129 samples were removed from the medium and dried under vacuum at room temperature to a
130 constant mass [15].

131 *2.5. Aerobic composting test*

132 Standardized laboratory-scale composting tests were conducted on 10.21 ± 2 g of molded PBAT
133 films containing 6.27 g of carbon (C) equal to 61.4 wt% of C based on elemental analysis (Vario
134 EL III apparatus, Elementar, Germany). Samples were analyzed before degradation and after
135 77 and 97 days of composting in a reactor system as described previously [22]. The mature
136 compost (502 ± 2 g with $79 \pm 0.2\%$ moisture), test samples, positive control (toilet paper), and
137 blanks were incubated in 4-liter poly(vinyl chloride) reactors (30×15 cm) placed in an
138 incubator (BioCold Environmental Inc., US) at 55 ± 0.5 °C. The test under simulated
139 composting conditions was performed following ASTM D5338-98 [23] equivalent to ISO
140 14852:2021 [24]. Compost inoculum (mixture of dairy manure and deciduous trees sawdust)
141 from a full-scale composting pile at the Ohio Agricultural Research and Development Center,
142 the Ohio State University, was aerated at 100 mL/min as described previously [25]. After 97
143 days, 68.7% of the C in the paper (positive control) was mineralized to CO₂, confirming active
144 decomposition.

145 *2.6. Anaerobic digestion test*

146 Process was conducted in laboratory-scale batch reactors with a 250 mL working volume. Each
147 reactor was filled with 200 g of active methanogenic inoculum according to ASTM D5511-02
148 [26] and ISO 15985:2014 [27] standards as described previously [22]. The inoculum was taken
149 from a commercial scale anaerobic digester on the Wooster campus of the Ohio State University
150 that treats municipal and commercial food processing wastes. Test samples ($m = 8.2 \pm 2$ g),

151 positive control (cellulose), and blanks were added to the batch reactors and incubated at $37 \pm$
152 $1 \text{ }^\circ\text{C}$ on an orbital shaker (at 115 rpm) for 30, 58, and 99 days. To maintain an anaerobic
153 atmosphere, each reactor was initially purged with nitrogen [26].

154 *2.7. Microscopic observation of the PBAT-based film's surface changes*

155 Surface morphology of the films before and after degradation was analyzed using various
156 microscopic techniques (OM, SEM, and AFM). OM images were obtained at $100 \times$
157 magnification using a Zeiss optical polarizing microscope (Opton-Axioplan, Germany)
158 equipped with a Nikon Coolpix 4500 digital camera (Japan). SEM observations were performed
159 with a Quanta 250 FEG (FEI Company, US) high-resolution environmental scanning electron
160 microscope at 5 kV, under low vacuum (80 Pa), and without coating using a secondary electron
161 detector (Large Field detector). AFM (Dimension ICON equipped with a NanoScope V
162 controller, Bruker Corporation, US) imaging was carried out in tapping mode in air utilizing a
163 standard $125 \text{ }\mu\text{m}$ long and $10\text{--}15 \text{ }\mu\text{m}$ high tip and a single-crystal doped silicon cantilever with
164 a flexural stiffness of $10\text{--}130 \text{ N m}^{-1}$ (Model PPP-NCH 10, NANOSENSORS, Switzerland).
165 Images were obtained with a piezoelectric scanner having a nominal size of $85 \text{ }\mu\text{m} \times 85 \text{ }\mu\text{m}$ and
166 recorded using NanoScope Analysis 1.9 Software (Bruker Corporation, US). AFM images were
167 acquired at scan areas of 2, 5, 10, 20, 40, and $90 \text{ }\mu\text{m}^2$. Representative images were selected from
168 three independent measurements performed on multiple samples. The microscopic images were
169 selected to best reflect the effect of RM- β -CD addition and its influence on qualitative and
170 quantitative changes in the surfaces before and after degradation, as well as to reflect the
171 differences in the hydrolytic degradation and biodegradation occurring.

172 *2.8. Gel permeation chromatography analysis*

173 The mass-average molar mass (M_w) of the PBAT-based films was estimated by GPC
174 experiments conducted in a chloroform solution at $35 \text{ }^\circ\text{C}$ and a flow rate of $1 \text{ mL}\cdot\text{min}^{-1}$ using a
175 set of two PL-gel $5 \text{ }\mu\text{m}$ MIXED-C ultrahigh efficiency columns (Polymer Laboratories, UK)

176 with a mixed bed and a linear range of $M_w = 200\text{--}2\,000\,000\text{ g}\cdot\text{mol}^{-1}$. A Nexera HPLC/UHPLC
177 Pump – LC-40DXR (Shimadzu, Japan) as the solvent delivery system with a Shodex SE 61
178 refractive index detector. A 10 μl volume of the sample solutions in chloroform (0.5% w/v) was
179 injected into the system. Polystyrene standards with low dispersity were used to generate a
180 calibration curve. The experimental error of the molar mass determined by the GPC method
181 was estimated to be $\pm 4\text{--}8\%$, which falls within the typical measurement uncertainty ($\pm 5\text{--}10\%$).
182 Therefore, for hydrolytic degradation at 37 °C, only the results obtained after 70 days were
183 considered, as earlier changes fell within the experimental error range.

184 *2.9. Nuclear magnetic resonance spectroscopy*

185 The ^1H NMR spectra of PBAT-base film samples were recorded at 600 MHz with a Bruker
186 Avance II Ultrashield Plus Spectrometer (Bruker BioSpin GmbH, Rheinstetten, Germany)
187 using a 5 mm sample tube. Dried deuterated chloroform was used as the solvent, and
188 tetramethylsilane was used as the internal standard at ambient temperature. All ^1H NMR spectra
189 were acquired with 64 scans, a 2.66 s acquisition time, and an 11 μs pulse width.

190 *2.10. Differential scanning calorimetry*

191 The thermal behavior of PBAT-based film was conducted using a non-modulated differential
192 scanning calorimeter (TA Instruments DSC Q2000, US). To obtain DSC curves, samples were
193 heated from -50 °C to 200 °C at a rate of $20\text{ °C}\cdot\text{min}^{-1}$.

194 *2.11. X-Ray diffraction analysis*

195 XRD studies were performed using the D8 Advance diffractometer (Bruker, Germany) with
196 Cu-K α cathode ($\lambda = 1.54\text{ \AA}$) operating at 40 kV voltage and 40 mA current. The scan rate was
197 $2.4^\circ\cdot\text{min}^{-1}$ with scanning step 0.02° in range of 5° to $80^\circ 2\Theta$. Identification of fitted phases was
198 performed using DIFFRAC.EVA program with the use of the International Centre for
199 Diffraction Data (ICDD) database. Crystallinity degrees (X_c) of polymer samples were
200 calculated using the peak decomposition method. The experimental error of the crystallinity

201 degree determined by the XRD method was estimated at $\pm 1\text{--}5\%$, which falls within the typical
202 measurement error range ($\pm 2\text{--}5\%$).

203 *2.12. Thermogravimetric analysis*

204 Thermal stability of the PBAT-based films was evaluated by the thermal analyzer TGA/DSC1
205 Mettler-Toledo (Columbus, OH, US) in nitrogen ($60\text{ mL}\cdot\text{min}^{-1}$) with a heating rate of 10
206 $^{\circ}\text{C}\cdot\text{min}^{-1}$. Mettler-Toledo AG StarSystem SW 9.30, Schwerzenbach, Switzerland was used to
207 generate a particular set of results.

208 **3. Results and Discussion**

209 Changes in the properties of PBAT-based films under conditions relevant to industrial solid-
210 waste management systems were evaluated through a series of controlled degradation
211 experiments in three environments for samples fabricated using three different methods. During
212 these experiments, PBAT-based films were degraded in aqueous environments at 37 and $70\text{ }^{\circ}\text{C}$
213 for 70 days, under aerobic composting conditions for 97 days, and under an anaerobic digestion
214 system for 99 days. Tests under aerobic composting and anaerobic digestion conditions were
215 used as models of organic recycling under industrial conditions, with reference to degradation
216 in aquatic environments. The use of different fabrication methods allowed assessment of the
217 films' physicochemical and degradation properties depending on the chosen method.
218 Furthermore, evaluating changes during degradation of samples with and without RM- β -CD
219 provided valuable data for comparing the degradation dynamics of the films in model industrial
220 systems with respect to the presence of the additive.

221 The sample lists with description and test conditions are specified in Table 1.

222

223 Table 1. Description of PBAT-based film samples used in this study.

Sample name	Sample type
EF	solvent-cast PBAT film before degradation

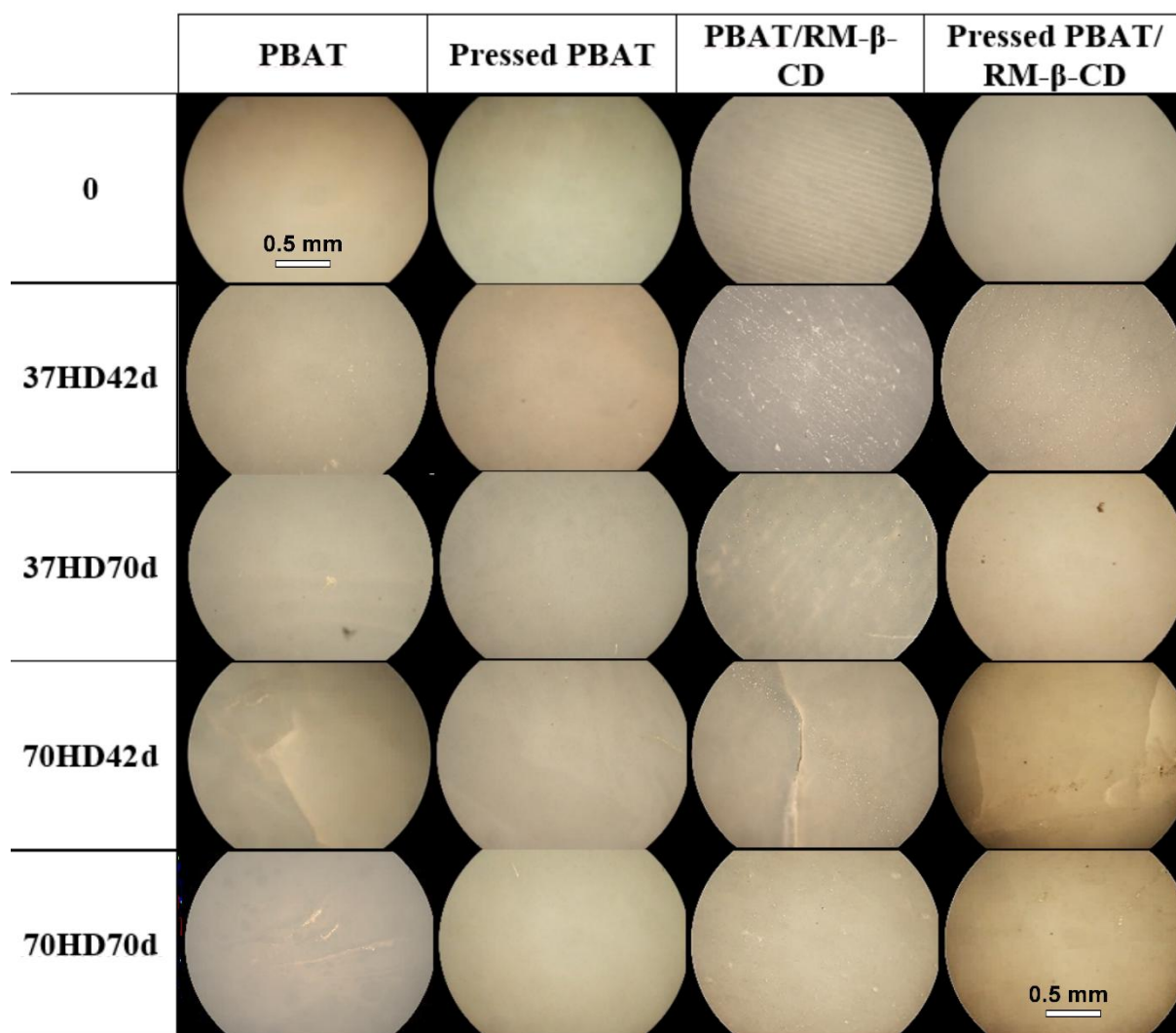
EF_37HDxd	solvent-cast PBAT film after x days of degradation in water at 37 °C
EF_70HDxd	solvent-cast PBAT film after x days of degradation in water at 70 °C
EFCD	solvent-cast PBAT film with RM- β -CD (solvent-cast PBAT/RM- β -CD)
EFCD_37HDxd	solvent-cast PBAT/RM- β -CD films after x days of degradation in water at 37 °C
EFCD_70HDxd	solvent-cast PBAT/RM- β -CD films after x days of degradation in water at 70 °C
PEF	pressed PBAT film before degradation
PEF_37HDxd	pressed PBAT film after x days of degradation in water at 37 °C
PEF_70HDxd	pressed PBAT film after x days of degradation in water at 70 °C
PEFCD	pressed PBAT film with RM- β -CD (pressed PBAT/RM- β -CD)
PEFCD_37HDxd	pressed PBAT/RM- β -CD after x days of degradation in water at 37 °C
PEFCD_70HDxd	pressed PBAT/RM- β -CD after x days of degradation in water at 70 °C
MEF	molded PBAT film before degradation
MEF_ACxd	molded PBAT film after x days of aerobic composting
MEF_ADxd	molded PBAT film after x days of anaerobic digestion

224 x – days of degradation: 7, 21, 42, and 70 for hydrolytic degradation, 77 and 97 for aerobic
225 composting; 30, 58, and 99 for anaerobic digestion

226

227 *3.1. Characterization of PBAT-based films and their properties during hydrolytic degradation*
228 *and biodegradation*

229 The surface morphology of the films before and after degradation was examined using OM,
230 SEM, and AFM. Figure 1 presents the optical microscopy images of PBAT-based films before
231 and after 42 and 70 days of incubation in water at 37 and 70 °C.



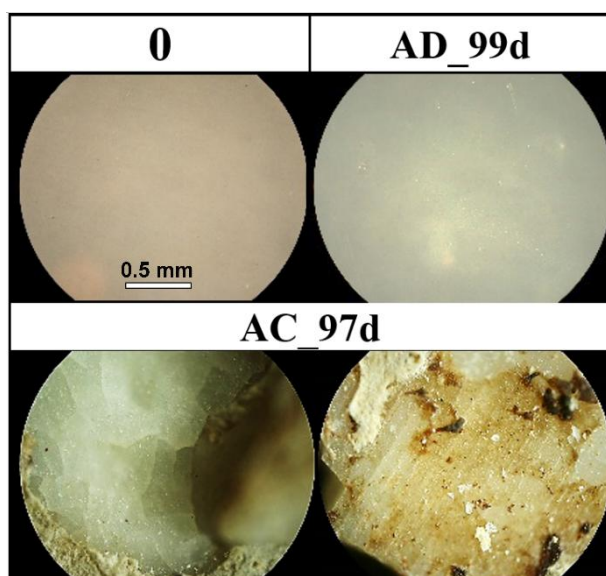
232

233 Figure 1. Representative optical microscopy micrographs of solvent-cast and pressed PBAT
 234 film surfaces illustrating morphological changes during hydrolytic degradation (HD). Images
 235 correspond to films before degradation (0) and after 42 and 70 days at 37 and 70 °C.
 236 Magnification: 100 ×.

237

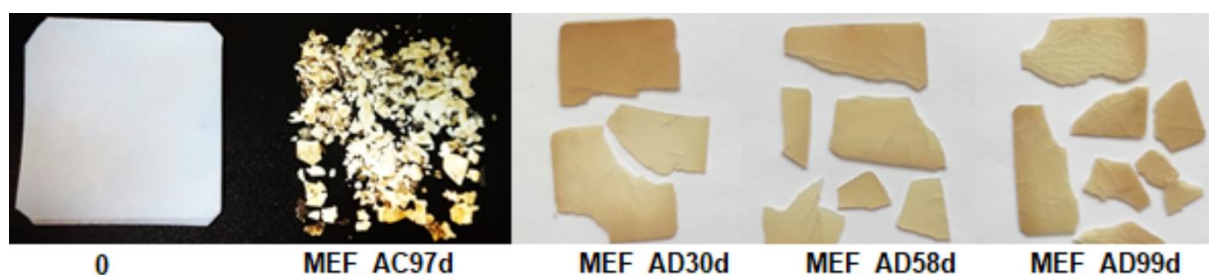
238 Microscopic observation showed that the surface of PBAT-based films before degradation was
 239 smooth and flat. After 42 and 70 days of incubation in water at 37 °C, no significant changes
 240 connected to the degradation process were observed (see 37HD42d and 37HD70d, Figure 1) on
 241 the surface of those PBAT-based films. However, for the PBAT films with RM- β -CD, grains
 242 began to appear after 42 days of degradation, which may indicate the nucleation process (see

243 37HD42d pressed PBAT/RM- β -CD film, Figure 1) [28]. After 42 days of incubation in water
244 at 70 °C, the surface of both solvent-cast films, and the pressed film with RM- β -CD, started to
245 crack (see 70HD42d, Figure 1). However, no evidence of disintegration was observed at a
246 macroscopic level during 70 days of hydrolytic degradation (data not shown). In the case of
247 molded PBAT films, during 97 days of incubation in compost, delamination and cracking
248 occurred across the entire surface, layer by layer. This was accompanied by the disintegration
249 of the material into small pieces (see molded PBAT films: AC_97d, Figures 2 and
250 MEF_AC97d, Figure 3).



251
252 Figure 2. Representative optical microscopy micrographs of molded PBAT film surfaces
253 illustrating morphological changes during degradation under model industrial conditions.
254 Images correspond to films before degradation (0), after 99 days of anaerobic digestion (AD),
255 and after 97 days of aerobic composting (AC). Magnification: 100 \times .

256

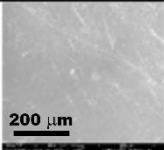
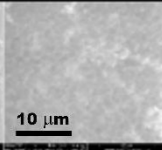
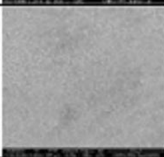
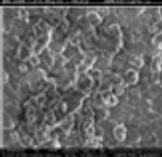
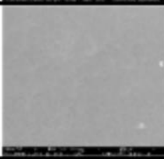
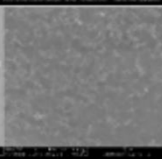
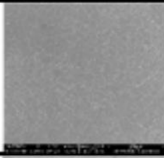
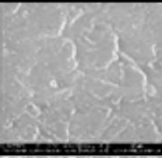
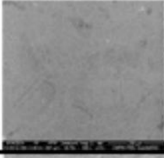
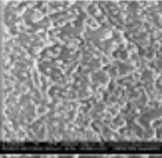
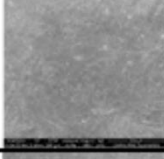
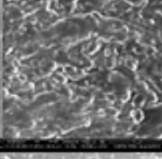
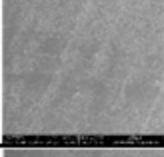
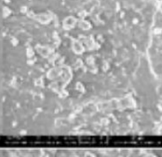
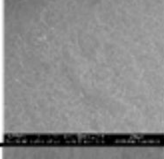
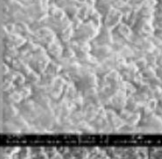
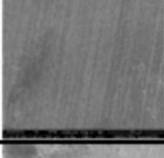
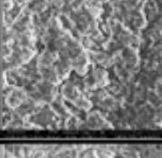
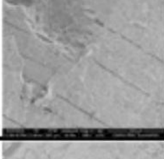
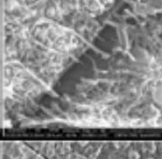
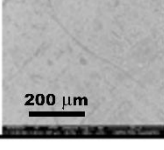
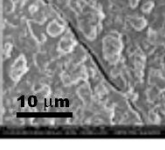


257

258 Figure 3. Representative digital images of molded PBAT films before degradation (0), after 97
259 days of aerobic composting (AC), and after 30, 58, and 99 days of anaerobic digestion (AD).
260 Abbreviations: EF – PBAT, M – molded.

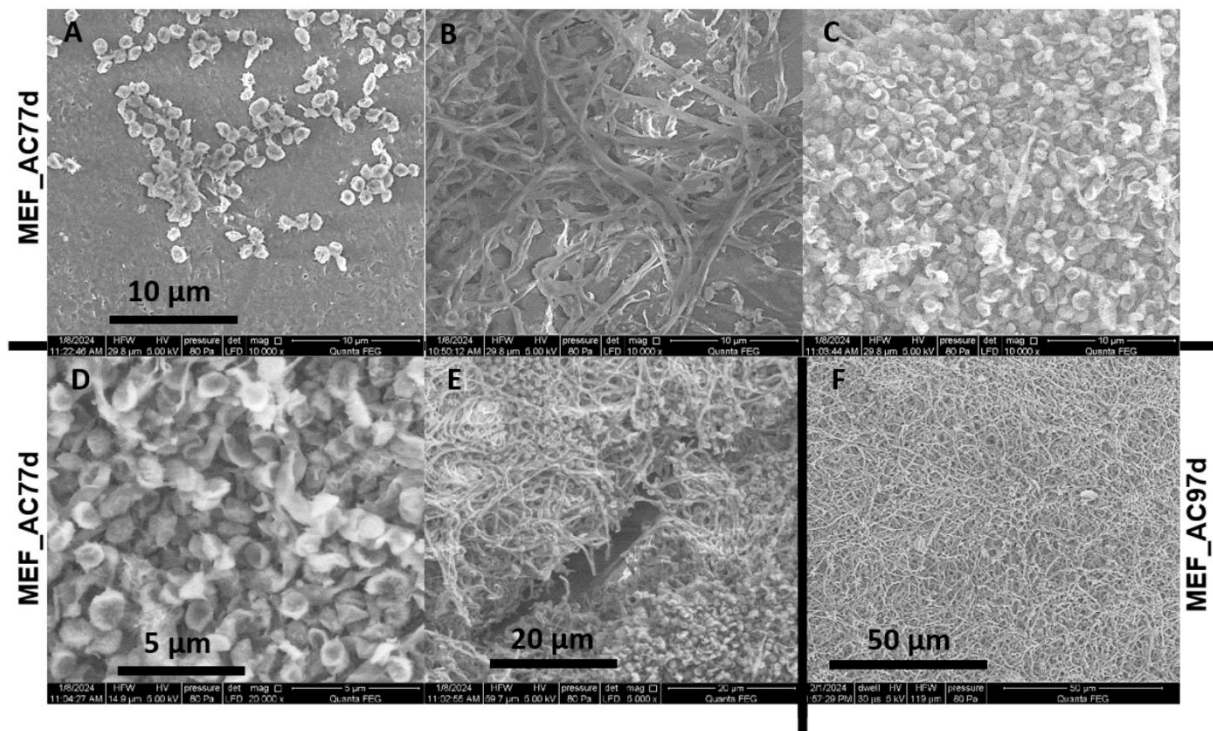
261

262 What is more, the homogeneous “licking” of the entire surface, layer by layer, indicates a
263 microbial hydrolysis (see molded PBAT: AC_97d, Figures 2). On the other hand, cracks on the
264 material surface, followed by erosion in its deeper parts, are more indicative of a water-
265 catalyzed hydrolysis mechanism [29]. Therefore, it can be said that both mechanisms contribute
266 to the degradation of PBAT-based films in the aerobic compost. In contrast, damage to the
267 surface of the molded PBAT film exposed to anaerobic digestion for 99 days was negligible
268 (see molded PBAT: AD_99d, Figure 2). In this case, mineralization was also low, and only
269 1.6% of the sample carbon was converted to CO₂ after 99 days of incubation. In addition, all
270 molded PBAT films disintegrated, which, given the anaerobic digestion with minor surface
271 damage, may indicate that simple hydrolysis with little biodegradation is the primary process
272 occurring in this environment (see MEF_AD30d, MEF_AD58d and MEF_AD99d, Figure 3).
273 The optical microscopy observations of the PBAT-based films were confirmed on the
274 micrometer scale by SEM analysis. Figure 4 shows SEM images of films before and after 42
275 days of incubation in water at 70 °C, as well as after 97 days of aerobic composting and 99 days
276 of anaerobic digestion.

Sample	Magnification	
	500 ×	10 000 ×
EF		
EF_70HD42d		
EFCD		
EFCD_70HD42d		
PEF		
PEF_70HD42d		
PEFCD		
PEFCD_70HD42d		
MEF		
MEF_AC97d		
MEF_AD99d		

278 Figure 4. Representative SEM images of PBAT-based film surfaces before degradation (0
279 days), after 42 days of hydrolytic degradation (HD) at 70 °C, after 97 days of aerobic
280 composting (AC), and after 99 days of anaerobic digestion (AD). Images were acquired at
281 magnifications of 500 × and 10,000 ×. Abbreviations: EF – PBAT, CD – RM-β-CD, P –
282 pressed, M – molded.

283
284 Before incubation, the surface of the solvent-cast films was smooth (see EF, 500 ×, Figure 4);
285 however, upon higher-magnification analysis at 10,000 × (scale of 10 μm) a more complex
286 surface morphology was revealed. The observed microstructure is consistent with literature
287 reports describing PBAT morphology with formation of β-form poly(1,4-butylene adipate)
288 (PBA) crystals, corresponding to the adipate segments of the PBAT copolymer. (see EF,
289 10,000 ×, Figure 4) [30,31]. The surface of pressed and molded films, compare to cast films,
290 prior to degradation was more heterogeneous due to the influence of polymer processing (see
291 PEF, PEFCD, MEF 10,000 ×, Figure 4). The most significant surface changes were noted in
292 the compost environment, where, following the incubation process, clear cracks and biofilm
293 could be seen on the molded PBAT films (see MEF_AC97d, Figure 4 and Figure 5).



294

295 Figure 5. Representative SEM images of biofilms on the surface of molded PBAT films after
 296 77 (A–E) and 97 (F) days of aerobic composting (AC). Images were acquired at the following
 297 magnifications: 20,000 × (D), 10,000 × (A–C), 5,000 × (E), and 2,500 × (F). Abbreviations: EF
 298 – PBAT, M – molded.

299

300 Cracks were also observed during anaerobic digestion, although they were not as distinct as
 301 those observed in the composting environment (see MEF_AD99d, Figure 4).

302 As degradation progressed, an increase in surface roughness was observed for all PBAT-based
 303 films, except for solvent-cast PBAT film (Table 2), as determined by AFM. Surface roughness
 304 was quantified using parameters such as the arithmetic mean deviation of the profile (R_a), which
 305 indicates the arithmetic mean of the absolute values of the profile heights calculated across the
 306 surface, and root mean square (RMS) of the profile heights (R_q), which is more sensitive to
 307 larger deviations from the mean plane.

308

309 Table 2. Surface roughness parameters obtained using AFM of solvent-cast and pressed PBAT
 310 films before degradation and after 70 days of hydrolytic degradation at 37 °C and 70 °C.

Sample	Solvent-cast PBAT film	Solvent-cast PBAT/RM- β - CD film	Pressed PBAT film	Pressed PBAT/RM- β - CD film
Before degradation				
R_a [nm]	42 \pm 5	208 \pm 16	118 \pm 9	114 \pm 10
R_q [nm]	53 \pm 4	281 \pm 29	152 \pm 6	167 \pm 7
Image Z range* [nm]	439 \pm 6	2357 \pm 316	1245 \pm 178	1492 \pm 190
After degradation at 37 °C				
R_a [nm]	36 \pm 5	217 \pm 26	198 \pm 5	186 \pm 5
R_q [nm]	46 \pm 4	302 \pm 14	235 \pm 8	228 \pm 8
Image Z range* [nm]	431 \pm 6	2846 \pm 355	1358 \pm 69	1456 \pm 69
After degradation at 70 °C				
R_a [nm]	365 \pm 61	473 \pm 94	310 \pm 446	156 \pm 21
R_q [nm]	452 \pm 76	599 \pm 109	378 \pm 534	198 \pm 21
Image Z range* [nm]	2971 \pm 817	4046 \pm 511	2519 \pm 2848	1687 \pm 163

311 * Image Z range corresponds to the maximum roughness

312

313 Incubation of the solvent-cast PBAT film at 37 °C for 70 days resulted in a slight decrease in
 314 roughness, which may be related to the initial leaching of basic components from the film (see
 315 Table 2 for the solvent-cast PBAT film before and after degradation at 37 °C). The other films

316 showed only minor changes under the same conditions (see image Z range of solvent-cast
 317 PBAT/RM- β -CD film, and R_a and R_q of pressed films before and after degradation at 37 °C,
 318 Table 2). On the other hand, after degradation at 70 °C, the roughness of the pressed films
 319 increased slightly (see pressed PBAT and PBAT/RM- β -CD films before and after degradation
 320 at 70 °C, Table 2). Likewise, the roughness of the solvent-cast films increased, especially those
 321 without RM- β -CD, where a 10-fold increase was observed (see R_a and R_q of solvent-cast PBAT
 322 films before and after degradation at 70 °C, Table 2).

323 This result is also confirmed by SEM images after 42 days of degradation at 70 °C (see
 324 EF_70HD42d and EFCD_70HD42d, Figure 4), where it was observed that surface damage
 325 progressed unevenly deeper into the material more strongly for the film without RM- β -CD (see
 326 EF_70HD42d, Figure 4). The pressed PBAT films before degradation were rough regardless of
 327 the addition of RM- β -CD. This could have been due to hot pressing and melting of the films
 328 during their preparation (see PEF, PEFCD, and MEF, Figure 4). A slight increase in roughness
 329 was observed upon degradation at 37 °C, in contrast to the solvent-cast PBAT film, where no
 330 increase was detected at this temperature. In the case of PBAT films degraded at 70 °C, a greater
 331 increase in roughness was observed compared to those degraded at 37 °C for all films, with the
 332 exception of pressed PBAT/RM- β -CD film (Table 2), where the film before degradation also
 333 had the lowest $X_c = 17\%$ (see PEFCD, Table 3).

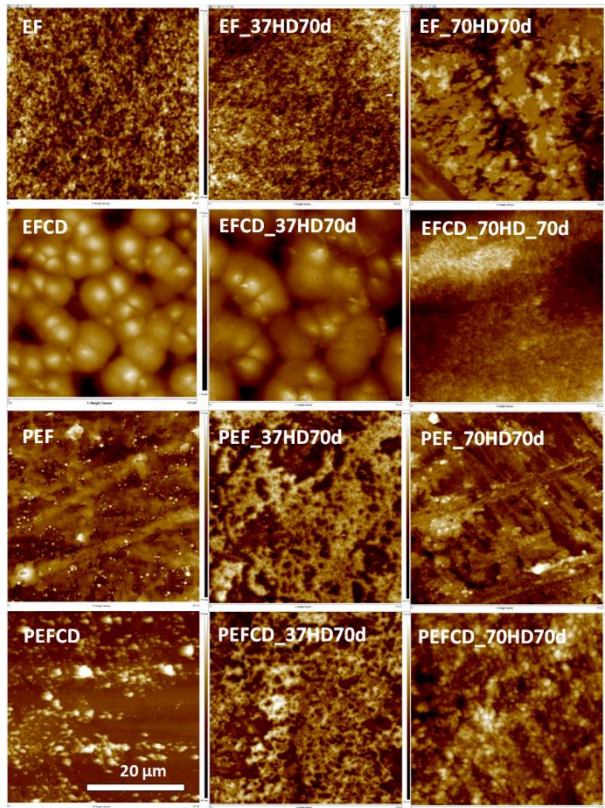
334
 335 Table 3. Crystallinity degrees of PBAT-based films determined by XRD. Data are shown for
 336 films before degradation, after 42 and 70 days of hydrolytic degradation (HD) at 70 °C, after
 337 97 days of aerobic composting (AC), and 99 days of anaerobic digestion (AD). Abbreviations:
 338 EF – PBAT, CD – RM- β -CD, P – pressed, M – molded.

Sample	Crystallinity degrees (X_c) [%]
EF	23

EF_70HD42d	29
EF_70HD70d	26
EFCD	27
EFCD_70HD42d	29
EFCD_70HD70d	27
PEF	27
PEF_70HD42d	28
PEF_70HD70d	27
PEFCD	17
PEFCD_70HD42d	27
PEFCD_70HD70d	23
MEF	28
MEF_AC97d	61
MEF_AD99d	33

339

340 Depending on the type of film and its processing, significant differences in the structure and
341 properties can be observed. AFM topographic images, for example, show dense morphology
342 with small PBAT microstructures [31] of solvent-cast films (see EF, Figure 6).



343

344 Figure 6. Representative AFM height images (scan size: $40 \times 40 \mu\text{m}$) of the solvent-cast and
 345 pressed PBAT film surfaces before degradation (first vertical row) and after 70 days of
 346 hydrolytic degradation at 37 and 70 °C. Abbreviations: EF – PBAT, CD – RM- β -CD, P –
 347 pressed.

348

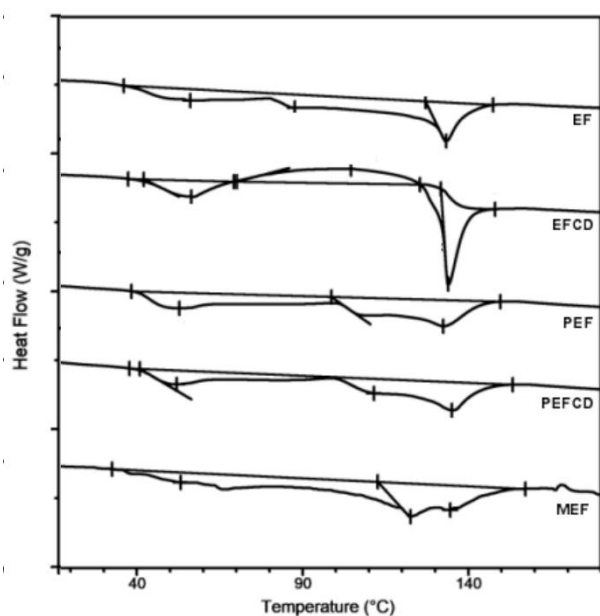
349 In contrast to solvent-cast PBAT/poly(lactide (PLA))-based film with phase separation [15], the
 350 solvent-cast PBAT film was characterized by a roughness that was approximately 15 times
 351 lower. The addition of RM- β -CD increased the roughness in the film, as evident in the AFM
 352 images (see EFCD, Figure 6). RM- β -CD is the nucleating agent here, which causes the
 353 formation of more nuclei in the matrix and increases the density of nucleation [28]. On the
 354 surface, well-resolved, large amounts of near-spherical agglomerates [32] were observed, with
 355 well-defined grain boundaries in the $\sim 5.9\text{--}13.4 \mu\text{m}$ size range and the highest surface roughness
 356 $R_a = 208 \text{ nm}$ (solvent-cast PBAT/RM- β -CD film before degradation, Table 2). This film was

357 also characterized by a higher crystallinity, $X_c = 27\%$ (see EFCD, Table 3), compared to the
358 neat solvent-cast PBAT film with $X_c = 23\%$ (see EF, Table 3).

359 A transcrystalline morphology was observed on the surface of this solvent-cast PBAT film with
360 RM- β -CD (see EFCD, Figure 6), in which a transcrystalline layer of PBAT was formed on the
361 RM- β -CD as a nucleating agent. PBAT is known for its relatively slow crystallization rate, but
362 can form transcrystalline layers, thin, highly oriented crystalline regions that form on the
363 polymer surface or on the surface of a nucleating agent, where the polymer crystallizes in a
364 highly oriented and surface-induced manner. These layers can significantly affect the
365 mechanical and barrier properties of the material [31]. Interestingly, for the pressed PBAT film
366 with RM- β -CD compared with the solvent-cast PBAT film with RM- β -CD, a reduction in
367 roughness was observed under the same conditions, with the lowest $X_c = 17\%$ (see pressed
368 PBAT/RM- β -CD and solvent-cast PBAT/RM- β -CD films before degradation, Table 2, and
369 PEFCD and EFCD, Table 3). Although nucleating agents are generally used to accelerate and
370 control crystallization, under certain conditions, particularly under high loading conditions, as
371 in the case of pressed PBAT film with RM- β -CD, they can also disrupt the crystallization
372 process [33]. AFM images (PEFCD, Figure 6) show that the pressed PBAT film with RM- β -
373 CD exhibits small, inhomogeneous grains, suggesting a more amorphous character [32].

374 In general, PBAT has a low degree of crystallinity with a melting temperature (T_m) of about
375 120–125 °C. Also, DSC analysis of PBAT may or may not show a cold crystallization
376 temperature (T_{cc}), depending on the specific copolymer and experimental conditions. Some
377 studies suggest that PBAT may not undergo a noticeable cold crystallization process, as was
378 observed in the study [34]. For the tested PBAT-based films before degradation, cold
379 crystallization phenomenon during the first heating run was observed only for the solvent-cast
380 PBAT film containing RM- β -CD ($T_{cc} = 104.6$ °C, $\Delta H_{cc} = 11.09$ J·g⁻¹) and for this film after 70
381 days of hydrolytic degradation at 37 °C ($T_{cc} = 99.1$ °C, $\Delta H_{cc} = 3.63$ J·g⁻¹). The exothermic peak

382 observed during the first heating run indicates that the addition of RM- β -CD alters the
 383 crystallization behavior and, as described above, promotes the formation of transcrystalline
 384 structures [31]. Cold crystallization was also observed for molded PBAT films after 77 days
 385 ($T_{cc} = 77.6$ °C, $\Delta H_{cc} = 4.22$ J·g⁻¹) and 97 days ($T_{cc} = 93.6$ °C, $\Delta H_{cc} = 2.75$ J·g⁻¹) of aerobic
 386 composting. After degradation, this phenomenon reflects an increase in chain mobility due to
 387 the decrease in molar mass and a reorganization of the polymer structure.
 388 The first heating run of the PBAT-based films shows a wide multimodal T_m range of 35–155
 389 °C for all the films with a sharp signal at $T_m = 133 \pm 2$ °C (Figure 7 and Table 4).



390
 391 Figure 7. Representative DSC thermograms of the solvent-cast, pressed (P), and molded (M)
 392 films showing the melting region (1-heating run). Abbreviations: EF – PBAT, CD – RM- β -CD.

393
 394 Table 4. Calorimetric parameters of PBAT-based films obtained at a heating rate of 20 °C·min⁻¹
 395 measured by DSC. Data are shown for films before degradation, after 42 and 70 days of
 396 hydrolytic degradation (HD) at 37 and 70 °C, after 97 days of aerobic composting (AC), and
 397 99 days of anaerobic digestion (AD). Abbreviations: EF – PBAT, CD – RM- β -CD, P – pressed,
 398 M – molded.

Sample	I-heating run		II-heating run after rapid cooling		
	T_m [°C]	ΔH_m [J·g ⁻¹]	T_g [°C]	T_m [°C]	ΔH_m [J·g ⁻¹]
Commercial PBAT pellet	65.2/96.0/12 8.1	34.97	-32.0	124.2 ^a	17.21 ^a
EF	56.2/87.3/13 3.3	27.16	-31.9	46.2/87.7/12 4.5	22.21
EF_37HD42d	54.1/75.0/89 .8/136.3	32.28	-33.6	92.9/122.0	30.13
EF_37HD70d	49.8/65.3/13 4.0	27.51	-34.0	122.5	20.89
EF_70HD42d	60.6/135.2	35.17	-36.3	60.6/138.4	35.05
EF_70HD70d	49.7/92.4/13 4.4/144.5	31.98	-35.6	130.4	21.93
EFCD	56.8/133.9	5.26/11.09	-25.1	121.3	21.18
EFCD_37HD42d	60.0/73.3/12 9.2	21.11	-31.0	125.7	24.38
EFCD_37HD70d	48.2/73.9/13 3.4	4.68/9.62	-29.5	124.7	20.32
EFCD_70HD42d	61.2/131.2	9.26/28.09	-36.4	143.9	29.67
EFCD_70HD70d	49.7/85.9/13 2.8	31.19	-27.5	133.2	22.41
PEF	52.8/132.4	29.75	-29.8	59.4/125.4	20.68
PEF_37HD42d	56.5/68.6/13 0.5/144.5	32.20	-34.2	125.3	22.64

PEF_37HD70d	46.7/63.0/12 8.8	35.65	-30.1	124.4	21.96
PEF_70HD42d	60.8/103.4/1 42.8/150.5	37.46	-39.1	56.5/116.0/1 35.5	26.72
PEF_70HD70d	53.6/99.9/13 6.1	30.14	-32.1	92.8/129.5	28.95
PEFCD	52.2/111.8/1 35.1	24.20	-30.1	44.0/124.8	18.97
PEFCD_37HD42d	51.5/65.7/82 .7/108.8/131 .5	29.32	-33.6	125.9	23.48
PEFCD_37HD70d	47.1/66.5/13 6.1	28.23	-28.4	31.7/126.0	22.09
PEFCD_70HD42d	59.0/98.3/12 2.7/145.0	44.20	-37.7	58.9/133.0	26.18
PEFCD_70HD70d	57.1/102.2/1 39.7	33.90	-34.3	50.5/123.0/1 37.9	24.74
MEF	53.1/66.9/12 3.3/134.5	34.18	-33.4	67.1/125.5	26.58
MEF_AC77d	127.9/148.3	18.13	-31.4	124.4/140.8	25.3
MEF_AC97d	67.5/115.4	21.96/80.88	-29.7	90.7/111.5 ^b	6.68/83.39 ^b
MEF_AD30d	53.0/73.7/13 0.2/132.5	29.92	-33.9	130.0	22.31

MEF_AD58d	13.6/66.8/11 6.2/132.0/13 6.8	40.0	-34.3	130.0	23.69
MEF_AD99d	75.5/108.1	49.98	-41.1	103.9	47.46

399 T_g – glass transition temperature, T_m – melting temperature, ΔH_m – melting enthalpy, ^a T_{cc} =

400 70.7 °C and ΔH_{cc} = 6.42 J·g⁻¹ in the II-heating run, ^b T_{cc} = 97.1 °C and ΔH_{cc} = 5.22 J·g⁻¹ in the

401 II-heating run.

402

403 The melting temperature of aliphatic 1,4-butylene adipate (BA) units, a component of the PBAT

404 copolymer, which varies depending on the crystal lattice structure, can be observed in the range

405 of 35–100 °C. The crystal lattice structure in PBAT depends, among others, on the arrangement

406 of soft BA units introduced into the rigid 1,4-butylene terephthalate (BT) units, which can form

407 co-crystallized or mixed crystal structures, leading to the formation of less perfect crystals and

408 crystal size reduction in relation to the homopolymer [35]. This results in a wide multimodal

409 melting temperature range for all films, both before and after degradation, except the solvent-

410 cast PBAT film with RM- β -CD. It should be emphasized that, before degradation, a T_{cc} was

411 observed only for solvent-cast PBAT film with RM- β -CD, as reflected in its distinct

412 morphology, clearly shown in the AFM images. (EFCD, Figure 6). T_{cc} can be observed in the

413 first heating run of a polymer with a transcrystalline morphology, particularly if the polymer

414 initially had a low degree of crystallinity. This occurs because transcrystalline structures, which

415 involve crystal growth oriented at the matrix-filler interface, can provide a nucleation site for

416 crystallization during the heating process. Even if the bulk polymer is not readily crystallized,

417 the presence of these structures could have induced crystallization during heating [36]. DSC

418 results show that for neat PBAT pressed film ΔH_m = 29.75 J·g⁻¹ (PEF, Table 4) was higher

419 compared to neat solvent-cast film (ΔH_m = 27.16 J·g⁻¹, see EF, Table 4). Furthermore, the

420 obtained XRD results indicated that both pressing and the addition of RM- β -CD to cast films
421 accelerated the crystallization of PBAT-based films (before degradation) from $X_c = 23\%$ for the
422 neat solvent-cast film (EF, Table 3) to $X_c = 27\%$ for both solvent-cast PBAT film with RM- β -
423 CD (EFCD, Table 3) and pressed film (PEF, Table 3). For the molded films, X_c was highest
424 reaching 28% (MEF, Table 3). Thus, the crystallinity of the tested films before degradation
425 depended on both the film fabrication method and the presence of additives [37].

426 The glass transition temperatures (T_g) from the second heating run, after rapid cooling to
427 remove the thermal history of the samples, were $-32\text{ }^\circ\text{C}$ for the pellet and solvent-cast PBAT
428 film (EF, Table 4). The addition of RM- β -CD caused an increase in the T_g to $-25\text{ }^\circ\text{C}$ (EFCD,
429 Table 4) because the addition of fine powder such as RM- β -CD to the polymer matrix resulted
430 in an increase in order due to nucleation, as in the case of pressing (except for pressed PBAT
431 films with RM- β -CD having the lowest $X_c = 17\%$, as discussed above). After incubation of the
432 samples in the tested environments, a decrease in T_g was observed. The slight increase in T_g
433 after incubation of the molded PBAT film in aerobic composting was due to a significant
434 increase in $X_c = 61\%$ after biodegradation (MEF_AC97d, Table 3 and 4). It is also worth noting
435 that the X_c values calculated from the XRD patterns using the peak deconvolution method show
436 a trend in crystallinity change consistent with the DSC results (see Table 3 and 4). Moreover,
437 PBAT as a copolymer can exhibit two distinct T_g . The presence of the different units (in this
438 case, butylene adipate and butylene terephthalate) can lead to microphase separation within the
439 polymer, where regions enriched in one monomer unit exist alongside regions enriched in the
440 other, resulting in two separate T_g . Unfortunately, due to the complex melting pattern of the
441 PBAT-based films in the second heating run, only one T_g was detected for the tested samples
442 [38].

443 PBAT-based films incubated in water for 42 days at $70\text{ }^\circ\text{C}$ exhibited a higher degree of
444 crystallinity than the samples before degradation, while a decrease in crystallinity was observed

445 after 70 days at 70 °C. Hydrolysis preferentially occurs first in the amorphous domains,
446 resulting in increased order and, consequently, an increase in the melting enthalpy (ΔH_m , see
447 Table 4). This is because the disordered arrangement of polymer chains in amorphous domains
448 facilitates enhanced water absorption. As a result, chain scission occurs, which leads to their
449 shortening. These chains have increased mobility and can organize more easily, leading to an
450 increase in the crystallinity of the polymer matrix. After a longer incubation time, water begins
451 to penetrate the crystalline part, and the degradation of crystalline domains begins, reducing the
452 crystallinity [39–41].

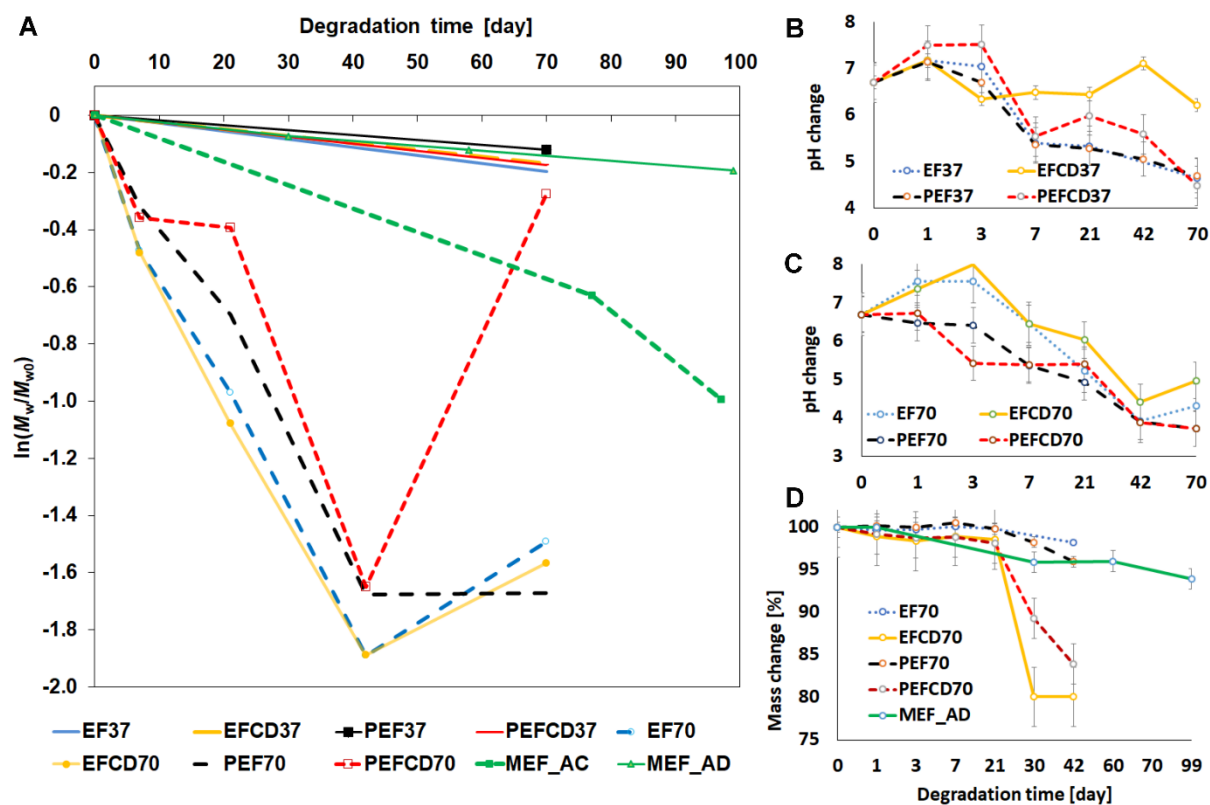
453 In the case of the molded PBAT films, the X_c value increased from 28% before the
454 biodegradation experiment to 33% following 99 days of anaerobic digestion. Furthermore, a
455 significant change in crystallinity was observed for the molded PBAT film after 97 days of
456 aerobic composting (the X_c value increased from 28% to 61%). A similar increase in
457 crystallinity was observed for the PBAT material after biodegradation at 55 °C, caused by the
458 assimilation of amorphous domains by microorganisms [42]. This explains the significant
459 increase in crystallinity and the greater share of microorganisms during 97 days of incubation
460 in aerobic composting compared to anaerobic digestion.

461 The results regarding the changes of morphology and thermal properties of PBAT-based films,
462 solvent-cast and pressed/molded, with and without the addition of RM- β -CD, occurring during
463 degradation, were discussed. The selection of samples allowed for the investigation of the
464 influence of RM- β -CD and the fabrication method on the degradation profile of PBAT-based
465 films. Hydrolytic degradation led to an initial increase in crystallinity, attributed to the
466 preferential degradation of amorphous domains, followed by a decrease after 70 days due to
467 degradation of less perfect crystalline regions. The results revealed that the incorporation of
468 RM- β -CD led to increased roughness in solvent-cast PBAT films. In contrast, pressed PBAT
469 films containing RM- β -CD exhibited reduced roughness under the same conditions, with the

470 lowest recorded crystallinity. Although nucleating agents are typically employed to enhance
471 and control crystallization, under certain conditions – particularly under high pressure, as in
472 pressing – they may also hinder the crystallization process. Before incubation, the solvent-cast
473 films exhibited a more complex surface structure, characteristic of PBAT morphology,
474 including the formation of β -form PBA crystals. As degradation progressed, the surface
475 roughness of all PBAT-based films increased, except for solvent-cast PBAT film incubated in
476 water at 37 °C, with the most notable changes observed in the compost environment, where a
477 distinct biofilm was observed following incubation. In summarizing the results of the
478 degradation tests, pressed PBAT-based films demonstrated greater stability in aqueous
479 environments compared to solvent-cast films. The results also show that after degradation in
480 environments containing microorganisms, the greatest damage was observed for the molded
481 PBAT film incubated in aerobic compost. A significant change in the crystallinity of molded
482 PBAT films was observed after 97 days of aerobic composting, due to the microbial
483 assimilation of amorphous domains – an effect not seen under anaerobic conditions. To confirm
484 these relationships, GPC, NMR, and TG analyses were performed.

485 *3.2. Assessment of the PBAT-based films' stability during the degradation process in selected* 486 *environments*

487 The molar mass and molar-mass dispersity of PBAT-based films during the incubation process
488 in water at 37 and 70 °C, as well as during aerobic composting and anaerobic digestion, have
489 been determined using the GPC analysis. The obtained results are presented in Figure 8A.



490

491 Figure 8. Degradation behavior of PBAT-based films: (A) Logarithm of the mass-
 492 average molar mass (M_w) to its initial value (M_{w0}) for solvent-cast, pressed, and molded films
 493 with and without RM- β -CD as a function of degradation time during hydrolytic degradation at
 494 37 and 70 °C, as well as during aerobic composting (AC) and anaerobic digestion (AD). (B)
 495 pH changes of the degradation medium during 70 days of hydrolytic degradation at 37 °C and
 496 (C) pH changes of the degradation medium during 70 days of hydrolytic degradation at 70 °C.
 497 (D) Mass change of PBAT-based films as a function of degradation time during 70 days of
 498 hydrolytic degradation at 70 °C. Abbreviations: EF – PBAT, CD – RM- β -CD, P – pressed, M
 499 – molded.

500

501 A continuous decrease in molar mass expressed as logarithm of the ratio of the mass-average
 502 molar mass (M_w) to its initial value (M_{w0}) ($\ln(M_w/M_{w0})$) of the PBAT-based films was observed
 503 during incubation in all environments, except for the degradation in water at 70 °C after 42
 504 days, as shown in Figure 8A (see EF70, EFCD70, PEF70, and PEFCD70). It is assumed that

505 until 42 days of hydrolytic degradation, the aliphatic (BA) segments in the copolymer chain
 506 degraded more rapidly, leaving less soluble aromatic (BT) segments, as also confirmed by
 507 NMR analysis after 42 days of degradation at 70 °C (compare EF and EF_70HD42d, EFCD
 508 and EFCD_70HD42d, PEF and PEF_70HD42d, PEFCD and PEFCD_70HD42d, Table 5). The
 509 residue with a higher molar mass (increase in molar mass expressed as $\ln(M_w/M_{w0})$) after 42
 510 days, see EF70, EFCD70, PEF70, and PEFCD70, Figure 8A and decrease in the number of BT
 511 units, compare EF_70HD42d and EF_70HD70d, EFCD_70HD42d and EFCD_70HD70d,
 512 PEF_70HD42d and PEF_70HD70d, PEFCD_70HD42d and PEFCD_70HD70d, Table 5) after
 513 70 days due to degradation of the aliphatic part, leaving rigid BT segments with lower
 514 solubility, in fact caused a decrease in visible units and a slower degradation rate. This is
 515 because the adipate ester linkages in PBA are more susceptible (more reactive) to hydrolysis
 516 compared to the terephthalate ester linkages in poly(1,4-butylene terephthalate) (PBT). This
 517 difference in reactivity is due to the presence of a more electron-withdrawing ester carbonyl
 518 group conjugated to an aromatic ring in the PBT structure, which makes the ester bond less
 519 susceptible to attack by water [43].

520

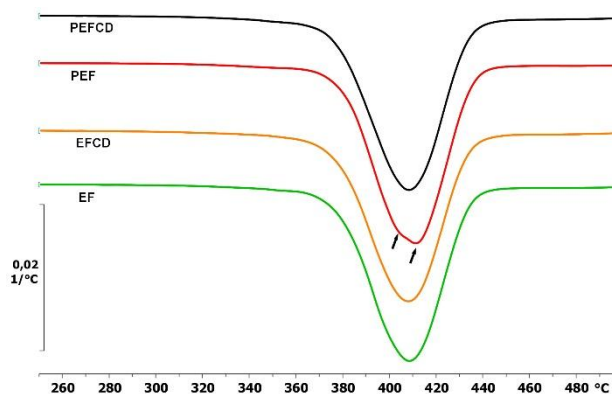
521 Table 5. Maximum mass loss rate determined by TGA and the BT/BA dyad sequence
 522 determined by ^1H NMR (based on ref. [44]) of solvent-cast, pressed (P) and molded (M) films
 523 before degradation, after 42 and 70 days of hydrolytic degradation (HD) at 37 and 70 °C, after
 524 77 and 97 days of aerobic composting (AC), and after 99 days of anaerobic digestion (AD).
 525 Abbreviations: EF – PBAT, CD – RM- β -CD.

Sample	BT/BA [mol%]	T_{max} [°C]
EF	48/52	408.5
EF_37HD70d	48/52	ND

EF_70HD42d	51/49	ND
EF_70HD70d	49/51	409.1
EFCD	48/52	408.2
EFCD_37HD70d	48/52	ND
EFCD_70HD42d	55/45	ND
EFCD_70HD70d	48/52	407.5
PEF	48/52	411.1
PEF_37HD70d	48/52	ND
PEF_70HD42d	49/51	ND
PEF_70HD70d	50/50	408.8
PEFCD	48/52	408.3
PEFCD_37HD70d	48/52	ND
PEFCD_70HD42d	50/50	ND
PEFCD_70HD70d	49/51	408.6
MEF	48/52	409.0
MEF_AC77d	53/47	407.2
MEF_AC97d	0*/100	402.0
MEF_AD30d	49/51	408.4
MEF_AD58d	48/52	408.4
MEF_AD99d	49/51	407.9

526 ND – No data/Not determined, T_{max} – the temperature of the maximum decomposition rate, BT
527 – 1,4-butylene terephthalate units of PBAT, BA – 1,4-butylene adipate units of PBAT, * not
528 completely dissolved
529

530 The influence of individual units of PBAT on the properties of the polymer matrix was also
531 observed in TGA thermograms (Table 5). It was found that the pressed PBAT film was
532 characterized by higher thermal stability before degradation at the temperature with the
533 maximum decomposition rate, $T_{max} = 411\text{ }^{\circ}\text{C}$ (see PEF, Table 5), than the other films with T_{max}
534 $= 408\text{ }^{\circ}\text{C}$ (see EF, EFCD, and PEFCD, Table 5 and Figure 9).



535
536 Figure 9. Representative DTG (derivative thermogravimetry) curves of solvent-cast, pressed
537 (P), and molded (M) PBAT films before degradation. Abbreviations: EF – PBAT, CD – RM-
538 β -CD.

539
540 Pressed neat PBAT film (see PEF, Figure 9) has a wider T_{max} signal, indicating separation
541 between BT and BA units, which may result in local changes in degradation rate. In this case,
542 microphase separation can occur, leading to incompatibility between components, which
543 dynamically form structures with separated phases in the micro- to nano-range due to
544 intramolecular phase separation. If the block lengths are appropriate, the two segments can be
545 separated into two phases. In random multiblock copolymers, long copolymer blocks are highly
546 segregated, while shorter blocks can penetrate “alien” domains and exchange between domains
547 and the interphase layer, which could be facilitated by the pressing process. Soft segments
548 characterized by greater conformational flexibility/weaker intermolecular interactions can also

549 penetrate hard segments that are more conformationally rigid or characterized by stronger
550 intermolecular interactions [45–47].

551 The degradation rate at both temperatures was slightly higher for solvent-cast PBAT-based
552 films, i.e., those with lower order (see EF37, EFCD37, EF70, and EFCD70, Figure 8A).
553 Interestingly, our previous studies of pressed PBAT/PLA films have demonstrated that the
554 incorporation of PLA to PBAT matrix does not accelerate hydrolytic degradation at 37 °C of
555 the PBAT/PLA blend compared with neat PBAT. At 37 °C, pressed PBAT films showed a
556 small decrease in molar mass expressed as $\ln(M_w/M_{w0})$ (see PEF37, Figure 8A), while in the
557 case of pressed PBAT/PLA films, no measurable loss of molar mass was observed after 70 days
558 [15]. At lower temperature even a moderate degree of polymer chain order can significantly
559 affect the degradation behavior.

560 It should be emphasized that, at the initial stage, the pH of the degradation medium increases
561 due to the leaching of basic components from the films, such as additives (e.g., stabilizers,
562 mineral fillers) or residual catalysts (Figure 8B). This is also consistent with the roughness
563 analysis, where a decrease in roughness was observed for the solvent-cast PBAT film incubated
564 at 37 °C for 70 days (see Table 2). Furthermore, at 37 °C, the pH of the degradation solution
565 drops faster for PBAT-based films without RM- β -CD (see EF37 and PEF37, Figure 8B), which
566 means a greater/faster leaching of degradation products from the polymer matrix for these films.
567 CDs can potentially interfere with the leaching of degradation products from the polymer matrix
568 by forming inclusion complexes, which can encapsulate the leaching oligomers and reduce their
569 mobility. At the same time, at 70 °C, a faster mass loss occurred for the solvent-cast PBAT film
570 with RM- β -CD (see EFCD70, Figure 8D), which in turn can be explained by higher roughness
571 (see solvent-cast PBAT/RM- β -CD film after degradation at 70 °C, Table 2), especially the
572 biggest maximum roughness (Image Z range) facilitating water penetration and disintegration,
573 which is also reflected in slightly lower thermal stability (see EFCD_70HD70d, Table 5).

574 The decrease in molar mass expressed as $\ln(M_w/M_{w0})$ in the case of degradation in compost
575 under aerobic conditions is half of that in the case of hydrolytic degradation at 70 °C (see
576 MEF_AC, Figure 8A), however, NMR showed only the presence of BT units of PBAT, which
577 may indicate the lack of solubility of the aromatic part and falsification of the actual molar mass
578 (see MEF_AC97d, Table 5). Whereas anaerobic digestion conditions result in low
579 biodegradation, which is confirmed by both the failure analysis (see molded PBAT: AD_99d,
580 Figure 2) and the slight decrease in molar mass expressed as $\ln(M_w/M_{w0})$ comparable to
581 hydrolytic degradation at 37 °C (see MEF_AD, Figure 8A). This observation is in line with the
582 results of PBAT bag degradation [48], where it was shown that this material was hardly
583 biodegradable under conventional conditions existing in anaerobic digestate at mesophilic
584 temperature (range between 20 and 45 °C). The observed differences in the behavior of PBAT-
585 based films, therefore, depend on the degradation environments and the presence or absence of
586 bacterial strains responsible for PBAT biodegradation, such as *Actinomucor elegans* [49].
587 Although the study does not include a direct analysis of microbial communities, the conclusions
588 regarding microbial involvement are based on indirect evidence, such as morphological changes
589 observed during degradation [22]. In general, biodegradation of the aromatic-aliphatic
590 copolymer PBAT occurs primarily through hydrolysis, with possible contributions from
591 microbial activity, which is consistent with the microscopic observation. Furthermore, it is well
592 known that hydrolytic degradation occurs more readily in amorphous domains than in
593 crystalline ones. In the amorphous/aliphatic part, water penetrates the polymer matrix more
594 easily, and hydrolytic degradation occurs more rapidly, with greater chain scission. The
595 observed decrease in molar masses expressed as $\ln(M_w/M_{w0})$ is consistent with a decrease in T_g
596 (as determined by DSC analysis) and indicates a gradual degradation resulting in the formation
597 of shorter polymer chains that act as plasticizers in the system. In contrast, the aromatic part
598 acts as a barrier to water, slowing down the hydrolytic degradation of the polymer matrix.

599 During aerobic composting, simple hydrolysis and biodegradation can occur simultaneously
600 [50,51]. Moreover, the increase in molar mass expressed as $\ln(M_w/M_{w0})$ indicates a change in
601 the properties of PBAT-based films due to the degradation of BA units and the amorphous
602 phase, and therefore the presence of a more stable crystalline phase and BT units in PBAT-
603 based films with lower solubility in CDCl_3 (deuterated chloroform for NMR analysis). A similar
604 phenomenon was observed in the case of poly(ethylene terephthalate) (PET), which is insoluble
605 in typical solvents; in this case, the degradation occurred depending on the distribution of
606 amorphous and crystalline domains throughout the polymer matrix [52].

607 A comprehensive analysis based on GPC, NMR, and TGA enabled the comparison of
608 degradation processes in PBAT-based films across different environments through the
609 evaluation of molar mass, compositional changes, and stability. During the 70 days of
610 hydrolytic degradation, no disintegration occurred despite significant degradation progress.
611 Under aerobic composting conditions, both microbial activity and hydrolysis contributed to the
612 degradation of the films. The reduced decrease in molar mass expressed as $\ln(M_w/M_{w0})$ at the
613 beginning of degradation (the degradation products immediately fall out of the polymer matrix)
614 and the delamination of the entire surface of the molded PBAT films after aerobic composting
615 are characteristic of biodegradation. In contrast, anaerobic digestion primarily involves simple
616 hydrolysis with a small share of biodegradation. The influence of individual PBAT copolymer
617 units on the degradation profile of the polymer matrix was also observed. This occurs because
618 the adipate ester linkages in PBA are more prone to hydrolysis than the terephthalate ester
619 linkages in PBT.

620 *3.3. Antimicrobial activity and in vitro cytocompatibility study*

621 Since the RM- β -CD/polymer mixture may exhibit antimicrobial activity [53], it was decided to
622 evaluate the antimicrobial properties of pressed PBAT films, both with and without the addition
623 of RM- β -CD, using the same methodology as in studies of PBAT/PLA-based films [15]. The

624 purpose of this analysis was to determine whether the incorporation of RM- β -CD affects the
 625 biological activity of the material, with potential applications in areas such as food packaging
 626 or biomedical products. The results revealed that pressed PBAT-based films did not exhibit any
 627 antimicrobial activity against the two pathogens tested: Gram-negative bacteria *E. coli* and
 628 Gram-positive bacteria *S. aureus*, as no inhibition zones were observed after 24 h of incubation,
 629 indicating these films lack antimicrobial properties (Table 6).

630

631 Table 6. Antimicrobial activity of PBAT and PBAT/RM- β -CD films.

Sample	<i>S. aureus</i> – zone of inhibition [mm]	<i>E. coli</i> – zone of inhibition [mm]
Pressed PBAT film	Not detected	Not detected
Pressed PBAT/RM- β -CD film	Not detected	Not detected
<i>Penicillin G</i> (control)	5.00 (\pm 1)	Not detected

632

633 A cytocompatibility test was performed using *in vitro* MTT assays. This was done to ensure the
 634 safety and environmental sustainability of pressed PBAT-based films (Table 7).

635

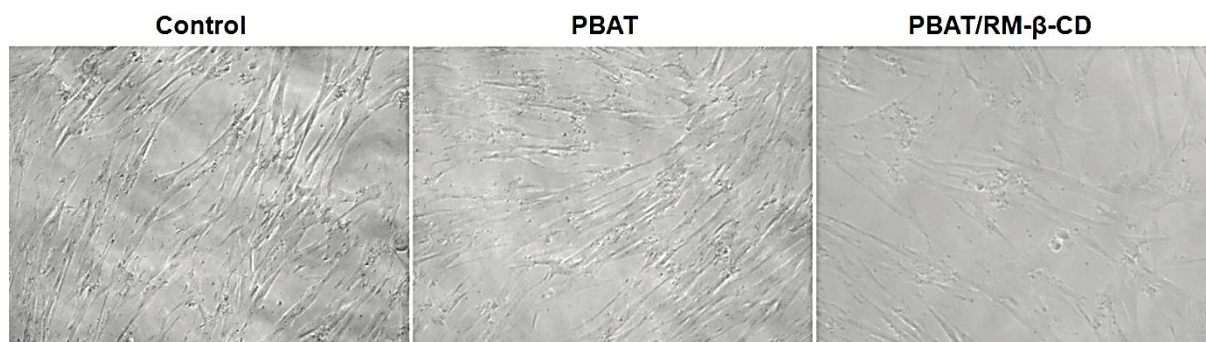
636 Table 7. MTT assay results following 24, 96 and 192 h of exposure to pressed PBAT and
 637 PBAT/RM- β -CD films.

Sample	Time [h]		
	24	96	192
	Mean cell viability [%]		

	Mean	Std. deviation	Mean	Std. deviation	Mean	Std. deviation
Pressed PBAT film	95.0	12.1	97.2	8.0	83.5	2.8
Pressed PBAT/RM- β -CD film	91.9	10.2	81.9	8.0	75.3	1.8

638

639 The pressed PBAT film showed a mean cell (MRC-5) viability of $95.0 \pm 12.1\%$ after 24 h
640 (Table 7), which is slightly lower, by 7%, than what was reported for the PBAT/PLA film
641 obtained by the same method [15]. The pressed PBAT film with the addition of RM- β -CD was
642 characterized by cytocompatibility of $91.9 \pm 10.2\%$ after the same time, which is also 7% less
643 than for the PBAT/PLA/RM- β -CD film. After 192 h, a decrease in cytocompatibility was
644 observed in both PBAT and PBAT/RM- β -CD films. Overall, the results indicate that the
645 addition of RM- β -CD may contribute to a decrease in cell viability similar to the use of PBAT
646 matrix alone, rather than the PBAT/PLA blend matrix. Morphological examination revealed no
647 changes in fibroblast morphology after 24 h of exposure (Figure 10).



648

649 Figure 10. *In vitro* cytocompatibility test results. Representative optical photomicrographs of
650 cells captured at $10 \times$ magnification after 24 h of exposure to pressed PBAT and PBAT/RM- β -
651 CD films.

652

653 4. Conclusion

654 The growth of the eco-friendly packaging market stems from both regulatory pressures and
655 consumer expectations, which increasingly emphasize biodegradability, recycled materials,
656 minimalism, and reuse. PBAT is of particular interest in this context, as it is a versatile and
657 biodegradable polymer that can be broken down under natural conditions through both
658 hydrolysis and microbial activity. This study examined the degradation of PBAT films during
659 aerobic composting, anaerobic digestion, and hydrolytic degradation, with a particular focus on
660 systematically analyzing alterations in surface morphologies and stability of PBAT-based films.
661 Both solvent-cast and pressed films with and without the presence of RM- β -CD, as well as
662 molded films, were examined.

663 The results indicate that the PBAT degradation behavior can be modified through tailoring the
664 composition of films and their fabrication methods, and adding appropriate green additives.
665 Additionally, studies on antimicrobial activity and cytotoxicity revealed no risks associated
666 with the potential applications of these materials.

667 In line with these findings, the results of this study confirm that incorporating RM- β -CD and
668 applying different film-fabrication methods do not compromise the suitability of PBAT-based
669 films for organic recycling. After use, these materials can be safely processed under industrial
670 conditions in accordance with EU directives. A clear understanding of their degradation
671 pathways is therefore essential, as it not only ensures compliance with solid-waste-management
672 requirements but also supports environmental protection by minimizing pollution.

673 **CRedit authorship contribution statement**

674 The manuscript was written through the contributions of all authors. All authors have given
675 their approval to the final version of the manuscript.

676 Author contributions:

677 Wanda Sikorska – Methodology, Resources, Investigation, Supervision, Writing – original
678 draft.

- 679 Khadar Duale – Resources, Investigation, Writing – review & editing.
- 680 Marta Musioł – Formal analysis, Writing – review & editing.
- 681 Henryk Janeczek – Formal analysis, Writing – review & editing.
- 682 Anna Hercog – Formal analysis.
- 683 Karolina Olszowska – Formal analysis.
- 684 Andrzej Marcinkowski – Formal analysis.
- 685 Silke Andrä-Żmuda – Formal analysis.
- 686 Marcin Godzierz – Formal analysis.
- 687 Marzena Pławszewska – Formal analysis.
- 688 Judit E. Puskas – Funding acquisition, Supervision.
- 689 Frederick C. Michel Jr. – Formal analysis, Investigation, Supervision.
- 690 Michael Klingman – Resources, Formal analysis.
- 691 Maria Letizia Focarete – Investigation, Writing – review & editing.
- 692 Mirosława El Fray – Methodology, Supervision, Funding acquisition.
- 693 Krzysztof Gorący – Resources, Investigation, Formal analysis.
- 694 Konrad Walkowiak – Investigation, Formal analysis.
- 695 Joanna Rokicka – Investigation.
- 696 Malwina Niedźwiedź – Investigation.
- 697 Iza Radecka – Methodology, Investigation, Formal analysis.
- 698 Abhishek Gupta – Methodology, Investigation, Formal analysis.
- 699 Marek Kowalczyk – Methodology, Funding acquisition, Writing – review & editing.
- 700 Joanna Rydz – Conceptualization, Methodology, Investigation, Supervision, Writing – original
701 draft, Writing – review & editing.
- 702 **Acknowledgment**

703 This work was supported by the European Union’s Horizon 2020 research and innovation
704 programme under the Marie Skłodowska-Curie grant agreement No 872152, project GREEN-
705 MAP, an international project co-financed by the program of the Minister of Science and Higher
706 Education entitled “PMW” in the years 2020–2024, contract No. 5092/H2020/2020/2 and Joint
707 Polish-Bulgarian project under the agreement on scientific cooperation between the Polish
708 Academy of Sciences and Bulgarian Academy of Sciences, “Tailor-made green polymer
709 systems for advanced medical and packaging applications”. Ms. Nina Stefaniak is
710 acknowledged for her help with the biodegradation tests. The authors also gratefully
711 acknowledge funding from USDA-NIFA, including HATCH Multi-State project W4045:
712 Agrochemical impacts on human and environmental health: Mechanisms and mitigation, and
713 HATCH project number OHO01417, as well as startup funds from the Ohio State University
714 #11232011000-11-PUSKAS. The use of the composting facility belonging to the lab of
715 Professor Fred Michel of OSU is greatly appreciated.

716 **Reference**

- 717 [1] I. Wojnowska-Baryła, D. Kulikowska, K. Bernat, 2020. Effect of bio-based products on
718 waste management, *Sustainability*. 12, 2088, <https://doi.org/10.3390/su12052088>.
- 719 [2] T.D. Moshood, G. Nawanir, F. Mahmud, F. Mohamad, M.H. Ahmad, A. Abdul Ghani,
720 2022. Sustainability of biodegradable plastics: New problem or solution to solve the global
721 plastic pollution?, *Curr. Res. Environ. Sustain.* 5, 100273,
722 <https://doi.org/10.1016/j.crgsc.2022.100273>.
- 723 [3] J. Kaushal, M. Khatri, S.K. Arya, 2021. Recent insight into enzymatic degradation of
724 plastics prevalent in the environment: A mini-review, *Cleaner Eng. Technol.* 2, 100083,
725 <https://doi.org/10.1016/j.clet.2021.100083>.
- 726 [4] W. Sikorska, M. Musioł, B. Zawidlak-Węgrzyńska, J. Rydz, Compostable polymeric
727 ecomaterials: environment-friendly waste management alternative to landfills, in: L.M.T.

728 Martínez, O.V. Kharissova, B.I. Kharisov (Eds.), Handbook of Ecomaterials, Springer
729 International Publishing AG, Cham, Switzerland, 2019, pp. 2733–2764.

730 [5] W. Sikorska, M. Musioł, Degradation principle and regulations, in: J. Rydz (Ed.),
731 Biodegradable Polymers: Value Chain in the Circular Economy, CRC Press, Boca Raton, 2023,
732 pp. 31–46.

733 [6] K. Nam, S.G. Kim, D.Y. Kim, D.Y. Lee, 2024. Enhanced mechanical properties of
734 polylactic acid/poly(butylene adipate-*co*-terephthalate) modified with maleic anhydride,
735 Polymers. 16(4), 518, <https://doi.org/10.3390/polym16040518>.

736 [7] Y.D. Hernandez-Charpak, H.J. Kansara, J.S. Lodge, N.C. Eddingsaas, C.L. Lewis, T.A.
737 Trabold, C.A. Diaz, Quantitative methodology for poly(butylene adipate-*co*-terephthalate)
738 (PBAT) microplastic detection in soil and compost, Environ. Sci. Pollut. Res. 33 (2025) 1755–
739 1764, <https://doi.org/10.1007/s11356-025-35978-4>.

740 [8] BASF, Ecoflex[®], BASF Performance Polymers. [https://plastics-](https://plastics-rubber.basf.com/global/en/performance_polymers/products/ecoflex)
741 [rubber.basf.com/global/en/performance_polymers/products/ecoflex](https://plastics-rubber.basf.com/global/en/performance_polymers/products/ecoflex), 2025 (accessed 10
742 January 2025).

743 [9] M. Musioł, W. Sikorska, H. Janeczek, W. Wałach, A. Hercog, B. Johnston, J. Rydz,
744 (Bio)degradable polymeric materials for a sustainable future – Part 1. Organic recycling of
745 PLA/PBAT blends in the form of prototype packages with long shelf-life, Waste Manage. 77
746 (2018) 447–454, <https://doi.org/10.1016/j.wasman.2018.04.030>.

747 [10] P. Singh, S. Kumar, Microbial enzyme in food biotechnology, in: M. Kuddus (Ed.),
748 Enzymes in food biotechnology, Elsevier, Oxford, UK, 2019, pp. 19–28,
749 <https://doi.org/10.1016/B978-0-12-813280-7.00002-5>.

750 [11] D.R. Patil, P.G. Ingole, K. Singh, D.S. Dalal, FTIR, ¹H NMR spectral, powder X-ray
751 diffraction and DSC studies of “β-cyclodextrin-para-chlorobenzonitrile” inclusion complex,
752 Res. J. Chem. Sci. 2 (2012) 60–63.

- 753 [12] E. Lizundia, F. Gómez-Galván, L. Pérez-Álvarez, L.M. León, J.L. Vilas, Poly(L-
754 lactide)/branched β -cyclodextrin blends: Thermal, morphological and mechanical properties,
755 Carbohydr. Polym. 144 (2016) 25–32, <https://doi.org/10.1016/j.carbpol.2016.02.043>.
- 756 [13] Y. Hao, Y. Chu, M. Zhang, W. Shi, Y. Chen, D. Li, L. Li, 2022. Preparation of functional
757 degradable antibacterial film and application in fresh-keeping of grass carp, J. Agric. Food Res.
758 9, 100341, <https://doi.org/10.1016/j.jafr.2022.100341>.
- 759 [14] J. Rydz, K. Duale, H. Janeczek, W. Sikorska, A. Marcinkowski, M. Musioł, M. Godzierz,
760 A. Kordyka, M. Sobota, C. Peptu, N. Koseva, M. Kowalczyk, 2022. Nematic-to-isotropic phase
761 transition in poly(L-lactide) with addition of cyclodextrin during abiotic degradation study, Int.
762 J. Mol. Sci. 23, 7693, <https://doi.org/10.3390/ijms23147693>.
- 763 [15] K. Duale, W. Sikorska, M. Musioł, H. Janeczek, M. Godzierz, A. Marcinkowski, M.
764 Kowalczyk, I. Radecka, A. Gupta, C. Peptu, J. Rydz, 2025. Randomly methylated β -
765 cyclodextrin as a modifier in PBAT/PLA-based films: Stability and crystallinity evaluation,
766 Polym. Degrad. Stab. 239, 111399, <https://doi.org/10.1016/j.polymdegradstab.2025.111399>.
- 767 [16] J. Rydz, W. Sikorska, M. Musioł, B. Zawidlak-Węgrzyńska, K. Duale, Sustainable future
768 alternative: (bio)degradable polymers for the environment, in: S. Hashmi, I.A. Choudhury
769 (Eds.), Encyclopedia of Renewable and Sustainable Materials, Elsevier, Oxford, 2020, pp. 274–
770 284.
- 771 [17] Y.X. Weng, Y.J. Jin, Q.Y. Meng, L. Wang, M. Zhang, Y.Z. Wang, Biodegradation
772 behavior of poly(butylene adipate-*co*-terephthalate) (PBAT), poly(lactic acid) (PLA), and their
773 blend under soil conditions, Polym. Test. 32 (2013) 918–926,
774 <https://doi.org/10.1016/j.polymertesting.2013.05.001>.
- 775 [18] W. Sikorska, P. Dacko, B. Kaczmarczyk, H. Janeczek, M. Domański, K. Mańczyk, M.
776 Kowalczyk, Synthesis and physicochemical properties of new (bio)degradable poly(ester-
777 urethane)s containing polylactide and poly[(1,4-butylene terephthalate)-*co*-(1,4-butylene

778 adipate)] segments, Polym. 52 (2011) 4676–4685,
779 <https://doi.org/10.1016/j.polymer.2011.08.015>.

780 [19] H. Janeczek, K. Duale, W. Sikorska, M. Godzierz, A. Kordyka, A. Marcinkowski, A.
781 Hercog, M. Musioł, M. Kowalczuk, D. Christova, J. Rydz, Poly(*L*-lactide) liquid crystals with
782 tailor-made properties toward a specific nematic mesophase texture, ACS Sustainable Chem.
783 Eng. 10 (2022) 3323–3334, <https://doi.org/10.1021/acssuschemeng.1c08282>.

784 [20] J. Rydz, K. Duale, W. Sikorska, M. Musioł, H. Janeczek, A. Marcinkowski, M. Siwy, G.
785 Adamus, P. Mielczarek, J. Silberring, J. Juszczuk, E. Piętka, I. Radecka, A. Gupta, M.
786 Kowalczuk, 2024. Oligopeptide-based molecular labelling of (bio)degradable polyester
787 biomaterials, Int. J. Biol. Macromol. 268, 131561,
788 <https://doi.org/10.1016/j.ijbiomac.2024.131561>.

789 [21] ISO 13781:2017, *Implants for surgery – Homopolymers, copolymers and blends on*
790 *poly(lactide) – In vitro degradation testing*, International Organization for Standardization,
791 Geneva, Switzerland.

792 [22] J. Rydz, K. Duale, M. Musioł, H. Janeczek, A. Hercog, A. Marcinkowski, K. Molnar, F.C.
793 Michel Jr, M. Klingman, M.L. Focarete, J.E. Puskas, P. Mielczarek, P. Suder, M. El Fray, K.
794 Walkowiak, J. Rokicka, M. Niedźwiedź, A. Grundmann, S.T. Kaysser, S. Detjen, B. Johnston,
795 I. Radecka, V. Kannappan, M. Kowalczuk, Assessing label stability in oligopeptide-modified
796 polymer filament for advanced materials: Ultraviolet exposure and biodegradation study, ACS
797 Sustainable Chem. Eng. 13 (2025) 14873–14892,
798 <https://doi.org/10.1021/acssuschemeng.5c04602>.

799 [23] ASTM D5338-98:2003, *Standard test method for determining aerobic biodegradation of*
800 *plastic materials under controlled composting conditions*, ASTM International, West
801 Conshohocken, PA, USA.

- 802 [24] ISO 14852:2021, *Determination of the ultimate aerobic biodegradability of plastic*
803 *materials in an aqueous medium – Method by analysis of evolved carbon dioxide*, International
804 Organization for Standardization, Geneva, Switzerland.
- 805 [25] E.F. Gómez, F.C. Michel Jr, Biodegradability of conventional and bio-based plastics and
806 natural fiber composites during composting, anaerobic digestion and long-term soil incubation,
807 *Polym. Degrad. Stab.* 98 (2013) 2583–2591,
808 <https://doi.org/10.1016/j.polymdegradstab.2013.09.018>.
- 809 [26] ASTM D5511-02:2002, *Standard test method for determining anaerobic biodegradation*
810 *of plastic materials under high-solids anaerobic-digestion conditions*, ASTM International,
811 West Conshohocken, PA, USA.
- 812 [27] ISO 15985:2014, *Plastics – Determination of the ultimate anaerobic biodegradation under*
813 *high-solids anaerobic-digestion conditions – Method by analysis of released biogas*,
814 International Organization for Standardization, Geneva, Switzerland.
- 815 [28] K. Tang, S. Wang, H. Liu, C. Zhang, Y. Yao, S. Lu, X. Liao, Manipulation of
816 crystallization nucleation and mechanical properties of PBAT films by octadecylamine-
817 cellulose, *ACS Sustainable Chem. Eng.* 12 (2024) 4276–4285,
818 <https://doi.org/10.1021/acssuschemeng.3c08384>.
- 819 [29] J. Rydz, A. Šišková, A. Andicsová Eckstein, 2019. Scanning electron microscopy and
820 atomic force microscopy: Topographic and dynamical surface studies of blends, composites,
821 and hybrid functional materials for sustainable future, *Adv. Mater. Sci. Eng.* 2019, 6871785,
822 <https://doi.org/10.1155/2019/6871785>.
- 823 [30] Z. Gan, H. Abe, Y. Doi, Temperature-induced polymorphic crystals of poly(butylene
824 adipate), *Macromol. Chem. Phys.* 203 (2002) 2369–2374,
825 <https://doi.org/10.1002/macp.200290007>.

- 826 [31] C. Zhou, K. Chen, Z.H. Zhang, M.F. Jing, C.T. Liu, C.Y. Shen, Y.M. Wang, Enhanced
827 crystallization of poly(butylene adipate-*co*-terephthalate) by a self-assembly nucleating agent,
828 Chin. J. Polym. Sci. 42 (2024) 663–674, <https://doi.org/10.1007/s10118-024-3092-x>.
- 829 [32] V.S. Waman, A.M. Funde, M.M. Kamble, M.R. Pramod, R.R. Hawaldar, D.P.
830 Amalnerkar, V.G. Sathe, S.W. Gosavi, S.R. Jadkar, 2011. Hydrogenated nanocrystalline silicon
831 thin films prepared by hot-wire method with varied process pressure, J. Nanotechnol. 2011,
832 242398, <https://doi.org/10.1155/2011/242398>.
- 833 [33] P. Gao, S. Alanazi, D. Masato, 2024. Crystallization of polylactic acid with organic
834 nucleating agents under quiescent conditions, Polymers. 16, 320,
835 <https://doi.org/10.3390/polym16030320>.
- 836 [34] O. Çoban, M.Ö. Bora, T. Kutluk, G. Özkoç, 2018. Mechanical and thermal properties of
837 volcanic particle filled PLA/PBAT composites, Polym. Compos. 39, E1500–E1511,
838 <https://doi.org/10.1002/pc.24393>.
- 839 [35] S. Su, M. Duhme, R. Kopitzky, 2020. Uncompatibilized PBAT/PLA blends:
840 manufacturability, miscibility and properties, Materials. 13, 4897,
841 <https://doi.org/10.3390/ma13214897>.
- 842 [36] M. Hao, H. Wu, F. Qiu, X. Wang, 2018. Interface bond improvement of sisal fibre
843 reinforced polylactide composites with added epoxy oligomer, Materials. 11, 398,
844 <https://doi.org/10.3390/ma11030398>.
- 845 [37] A.R. de Matos Costa, A. Crocitti, L. Hecker de Carvalho, S.C. Carroccio, P. Cerruti, G.
846 Santagata, 2020. Properties of biodegradable films based on poly(butylene succinate) (PBS)
847 and poly(butylene adipate-*co*-butylene terephthalate) (PBAT) blends, Polymers. 12, 2317,
848 <https://doi.org/10.3390/polym12102317>.
- 849 [38] M.C. Branciforti, C.F. Bellani, C.L. Morelli, A. Ferrand, N. Benkirane-Jessel, R.E.S.
850 Bretas, Poly(butylene adipate-*co*-terephthalate) and poly(ϵ -caprolactone) and their

851 bionanocomposites with cellulose nanocrystals: thermo-mechanical properties and cell viability
852 study, *J. Renew. Mater.* 7 (2019) 269–277, <https://doi.org/10.32604/jrm.2019.01833>.

853 [39] Y. Brito, M.A. Sabino, G. Ronca, A.J. Müller, Changes in crystalline morphology, thermal,
854 and mechanical properties with hydrolytic degradation of immiscible biodegradable
855 PPD_X/PCL blends, *J. Appl. Polym. Sci.* 110 (2008) 3848–3858,
856 <https://doi.org/10.1002/app.28883>.

857 [40] C.C. Chu, Hydrolytic degradation of polyglycolic acid: tensile strength and crystallinity
858 study, *J. Appl. Polym. Sci.* 26 (1981) 1727–1734, <https://doi.org/10.1002/app.1981.070260527>.

859 [41] A.D. Banjo, V. Agrawal, M.L. Auad, A.D.N. Celestine, 2022. Moisture-induced changes
860 in the mechanical behavior of 3D printed polymers, *Compos. Part C: Open Access.* 7, 100243,
861 <https://doi.org/10.1016/j.jcomc.2022.100243>.

862 [42] P. Svoboda, M. Dvorackova, D. Svobodova, Influence of biodegradation on crystallization
863 of poly(butylene adipate-*co*-terephthalate), *Polym. Adv. Technol.* 30 (2019) 552–562,
864 <https://doi.org/10.1002/pat.4491>.

865 [43] A. Bher, P.C. Mayekar, R.A. Auras, C.E. Schvezov, 2022. Biodegradation of
866 biodegradable polymers in mesophilic aerobic environments, *Int. J. Mol. Sci.* 23, 12165,
867 <https://doi.org/10.3390/ijms232012165>.

868 [44] M. Musioł, J. Rydz, H. Janeczek, A. Kordyka, J. Andrzejewski, T. Sterzyński, S. Jurczyk,
869 M. Cristea, K. Musioł, M. Kampik, M. Kowalczyk, 2022. (Bio)degradable biochar composites
870 – Studies on degradation and electrostatic properties, *Mater. Sci. Eng. B.* 275, 115515,
871 <https://doi.org/10.1016/j.mseb.2021.115515>.

872 [45] E.N. Govorun, A.V. Chertovich, 2017. Microphase separation in random multiblock
873 copolymers, *J. Chem. Phys.* 146, 034903, <https://doi.org/10.1063/1.4973933>.

874 [46] T.P. Balaji, S. Choudhury, Block copolymer phase separation basics, thermodynamics, and
875 applications in thermoplastic elastomers, in: N.K. Singha, S.C. Jana (Eds.), *Advances in*

876 Thermoplastic Elastomers, Elsevier, 2024, pp. 45–91, [https://doi.org/10.1016/B978-0-323-](https://doi.org/10.1016/B978-0-323-91758-2.00013-1)
877 [91758-2.00013-1](https://doi.org/10.1016/B978-0-323-91758-2.00013-1).

878 [47] C. Schaller, 4.6: Microphase separation, in: 4: Polymer Properties, The LibreTexts
879 libraries, <https://chem.libretexts.org/@go/page/190671?pdf>, 2026 (accessed 10 January 2026).

880 [48] S.J. Álvarez-Méndez, J.L. Ramos-Suárez, A. Ritter, J.M. González, Á.C. Pérez, 2023.
881 Anaerobic digestion of commercial PLA and PBAT biodegradable plastic bags: Potential
882 biogas production and ¹H NMR and ATR-FTIR assessed biodegradation, Heliyon. 9, e16691,
883 <https://doi.org/10.1016/j.heliyon.2023.e16691>.

884 [49] H. Jia, M. Zhang, Y. Weng, C. Li, 2021. Degradation of polylactic acid/polybutylene
885 adipate-*co*-terephthalate by coculture of *Pseudomonas mendocina* and *Actinomucor elegans*, J.
886 Hazard. Mater. 403, 123679, <https://doi.org/10.1016/j.jhazmat.2020.123679>.

887 [50] Y. Fu, G. Wu, X. Bian, J. Zeng, Y. Weng, 2020. Biodegradation behavior of poly(butylene
888 adipate-*co*-terephthalate) (PBAT), poly(lactic acid) (PLA), and their blend in freshwater with
889 sediment, Molecules. 25, 3946, <https://doi.org/10.3390/molecules25173946>.

890 [51] J. Jian, Z. Xiangbin, H. Xianbo, An overview on synthesis, properties and applications of
891 poly(butylene-adipate-*co*-terephthalate)-PBAT, Adv. Ind. Eng. Polym. Res. 3 (2020) 19–26,
892 <https://doi.org/10.1016/j.aiepr.2020.01.001>.

893 [52] J. Yu, D. Zhou, W. Chai, B. Lee, S. Lee, J. Yoon, M. Ree, Synthesis and non-isothermal
894 crystallization behavior of poly(ethylene-*co*-1,4-butylene terephthalate)s, Macromol. Res. 11
895 (2003) 25–35, <https://doi.org/10.1007/BF03218274>.

896 [53] S. Das, Z. Gazdag, L. Szente, M. Meggyes, G. Horváth, B. Lemli, S. Kunsági-Máté, M.
897 Kuzma, T. Kőszegi, Antioxidant and antimicrobial properties of randomly methylated β-
898 cyclodextrin-captured essential oils. Food Chem. 278 (2019) 305–313,
899 <https://doi.org/10.1016/j.foodchem.2018.11.047>.